Volume II:

Field Implementation of Super-Workable Fiber-Reinforced Concrete for Infrastructure Construction

Participating Consortium Member:
Missouri University of Science and Technology
Polytechnic Institute of New York University
Rutgers, The State University of New Jersey
University of Oklahoma

Authors:
Kamal H. Khayat, Ph.D., P.Eng.
Ahmed Abdelrazik, Ph.D. Candidate

RE-CAST:
REsearch on Concrete Applications for Sustainable Transportation
Tier 1 University Transportation Center

DISCLAIMER

The contents of this report reflect the views of the authors, who are responsible for the facts and the accuracy of the information presented herein. This document is disseminated under the sponsorship of the U.S. Department of Transportation's University Transportation Centers Program, in the interest of information exchange. The U.S. Government assumes no liability for the contents or use thereof.

TECHNICAL REPORT DOCUMENTATION PAGE

1. Report No. RECAST UTC # 00046732	2. Government Accession No.	3. Recipient's Catalog No.
4. Title and Subtitle Volume II: Field Implementation Of Super-Workable Fiber-Reinforced Concrete For Infrastructure Construction		**5. Report Date** January 2020
		6. Performing Organization Code:
7. Author(s) Kamal H. Khayat and Ahmed Abdelrazik		**8. Performing Organization Report No.** Project # 00046732
9. Performing Organization Name and Address RE-CAST – Missouri University of Science and Technology 500 W. 16th St., 223 ERL Rolla, MO 65409-0710		**10. Work Unit No.**
		11. Contract or Grant No. USDOT: DTRT13-G-UTC45
12. Sponsoring Agency Name and Address Office of the Assistant Secretary for Research and Technology U.S. Department of Transportation 1200 New Jersey Avenue, SE Washington, DC 20590		**13. Type of Report and Period Covered:** Final Report Period: 6/1/2014 – 12/31/2019
		14. Sponsoring Agency Code:

15. Supplementary Notes

The investigation was conducted in cooperation with the U. S. Department of Transportation.

16. Abstract

A fiber-reinforced super-workable concrete (FR-SWC) made with 0.5% micro-macro steel fibers and 5% CaO-based expansive agent was used for the new deck slab of Bridge A8509. The selected FR-SWC had a targeted slump flow of 20 in. at the casting location. Multiple trial batches were performed, in collaboration with the concrete supplier, to adjust the mixture composition to meet the targeted performance criteria. This was followed up by casting the fibrous concrete in a mock-up slab measuring 10×10 ft that was prepared to simulate the tight rebar and the roadway crown slope in the transverse direction. The results indicated the necessity to lower the concrete slump from the intended value for FR-SWC to hold the 2% crown slope of the bridge deck in the transverse direction. The final mixture that was selected following the trial batches and mock-up placement had a slump consistency of 8 ± 2 in. (FRC). Six sensor towers were installed in the slab within 18 ft to the East and West sides of the intermediate bent to monitor in-situ properties of the concrete. Each tower had three humidity sensors, three thermocouples, and 12 concrete strain gauges. The slump values varied between 6 and 10 in. Slump values were around 8.5 in. The fresh air volume ranged from 4.4% to 5.8%, and the concrete temperature ranged from 85 to 97 °F. At 56 days, the compressive strength ranged from 7,020 to 8,360 psi and had a mean value of 7,770 psi. Data up to 260 days are reported at the time of the preparation of this report. The in-situ concrete temperature was shown to increase around 45 oF during the first day, reaching a maximal temperature of 140 oF. The temperature then dropped to ambient temperature of approximately 95 oF during the second day. It then varied on a daily basis with the ambient temperature. The relative humidity of concrete ranged between 90% and 100% initially, then decreased with time until reaching approximate values of 80% to 85%. The loss of humidity was higher in magnitude and rate near the top surface of the bridge deck compared to the middle and bottom of the slab. A 3D finite element model (FEM) was developed to predict the top and bottom structural strain values in the concrete deck that can be developed due to the weight of the bridge. The estimated strain values were compared to those recorded by the in-situ sensors in the longitudinal and transverse directions. In the longitudinal direction, the stresses were shown to reach the maximum positive values at the points of contact of the girder with the concrete diaphragm. The values decreased gradually along the length of the bridge to reach the maximum negative values approximately at the mid-span of the bridge deck. The area under consideration, where the towers are located, was in complete tension in the longitudinal and transverse directions. The highest tensile strain values reached 2100 micro-strain at the intersection of the intermediate bent with one of the pre-cast concrete girders. A strain model was proposed to evaluate the strain data collected from the embedded sensors. The model represents the total strain as a summation of strains due to thermal deformation, drying and autogenous shrinkage, and structural deformation. The model was used to evaluate strains and estimate values of the concrete shrinkage during the first 30-36 hours, which corresponded to the time of demolding of the shrinkage samples as well as the load distribution factor between the concrete slab and the steel corrugated sheet that varied with concrete age. Findings indicated that the load distribution factor increased with concrete age reaching a value of 0.98 at 260 days. The concrete shrinkage during the first 30-36 hours was then estimated to be 75 micro-strain.

17. Key Words Bridge construction; Bridge members; Fiber reinforced concrete; Infrastructure; Performance based specifications; Self compacting concrete; Substructures; Superstructures; Workability	**18. Distribution Statement** No restrictions. This document is available to the public.	
19. Security Classification (of this report) Unclassified	**20. Security Classification (of this page)** Unclassified	**21. No of Pages** 86

Form DOT F 1700.7 (8-72)   Reproduction of form and completed page is authorized.

Field Implementation of Super-Workable

Fiber-Reinforced Concrete for Infrastructure Construction

Final Report

Investigators

Kamal H. Khayat, Ph.D., P.Eng., Professor, Missouri S&T
Ahmed Abdelrazik, Ph.D. Candidate Missouri S&T

COPYRIGHT STATEMENT

Authors herein are responsible for the authenticity of their materials and for obtaining written permissions from publishers or individuals who own the copyright to any previously published or copyrighted material used herein.

DISCLAIMER STATEMENT

The opinions, findings, and conclusions expressed in this document are those of the investigators. They are not necessarily those of the Missouri Department of Transportation, U.S. Department of Transportation, or Federal Highway Administration. This information does not constitute a standard or specification.

ACKNOWLEDGMENTS

EXECUTIVE SUMMARY

This report presents the results of a field implementation involving the use of highly flowable fiber-reinforced concrete (FRC) for the new deck slab of Bridge A8509 over Route 50 near Taos, Missouri. The two-span girder type bridge consists of four girders with span lengths measuring about 126 ft (38.4 m) and 115 ft (35.05 m) in length. The width of the bridge is 30 ft (9.14 m). The end bents and intermediate bent axes are skewed at 15 degrees to the axes of the girders.

A fiber-reinforced super-workable concrete (FR-SWC) made with 0.5% micro-macro steel fibers and 5% CaO-based expansive agent (EA) that can develop high tensile strength, low shrinkage, and high resistance to cracking was selected for the new deck slab of Bridge A8509. Although the concrete was intended for construction of bridge substructure elements, a decision was made to use it for the re-decking work given the anticipated high tensile stresses in the bridge deck at the intermediate bent and the relatively high concentration of steel reinforcement necessitating the use of a highly flowable fibrous mixture.

The selected FR-SWC had a targeted slump flow of 20 in. (508 mm) at the casting location. Multiple trial batches were performed, in collaboration with the concrete supplier, to adjust the mixture composition to meet the targeted performance criteria. This was followed up by casting the FRC in a mock-up slab measuring 10×10 ft (3.05×3.05 m) that was prepared to simulate the tight rebar and the roadway crown slope in the transverse direction. The results indicated the necessity to lower the concrete slump from the intended value for FR-SWC to hold the 2% crown slope of the bridge deck in the transverse direction. The final mixture that was selected following the trial batches and mock-up placement had a slump consistency of 8 ± 2 in. (203 ± 51 mm).

The casting of the FRC took place on July 26, 2017 between midnight and 7 am. In total, 40 concrete trucks delivered 330 yd^3 (252 m^3) of FRC. Given the high ambient and concrete temperatures, ice was used as partial replacement of the mixing water. Test samples were taken from seven of the concrete trucks to evaluate the workability, mechanical properties, and drying shrinkage of the FRC. All sampling took place at the end of the pumpline.

The slump values varied between 6 and 10 in. (152 and 254 mm). Slump values were more consistent after Truck #25 with approximate slump values of 8.5 in. (216 mm). The fresh air volume ranged from 4.4% to 5.8%, and the concrete temperature ranged from 85 to 97 °F (29 to 36 °C).

The 28-day compressive strength measured using 4 × 8 in. cylinders (102 × 203 mm) varied between 5,780 and 6,980 psi (39.9 to 48.1 MPa) and had a mean value of 6,450 psi (44.5 MPa). At 56 days, the compressive strength ranged from 7,020 to 8,360 psi (48.4 to 57.6 MPa) and had a mean value of 7,770 psi (53.6 MPa). The average 56-day flexural strength was 860 psi (5.9 MPa). The mean 3-day elastic modulus was 3,660 ksi (25.2 GPa), and the mean value at 56 days was 3,855 ksi (26.6 GPa).

The linear expansion of the control concrete prisms subjected to 7 days of moist curing reached a peak value of 125 micro-strain after 7 days. The average shrinkage values determined at 56 and 260 days of age were limited to 185 and 320 micro-strain, respectively.

Six sensor towers were installed in the slab within 18 ft (5.5 m) to the East and West sides of the intermediate bent to monitor in-situ properties of the concrete. Each tower had three humidity sensors, three thermocouples, and 12 concrete strain gauges. Data up to 260 days are reported at the time of the preparation of this report. The in-situ concrete temperature

was shown to increase around 45 $^{\circ}$F (25 $^{\circ}$C) during the first day, reaching a maximal temperature of 140 $^{\circ}$F (60 $^{\circ}$C). The temperature then dropped to ambient temperature of approximately 95 $^{\circ}$F (35 $^{\circ}$C) during the second day. It then varied on a daily basis with the ambient temperature.

The relative humidity of concrete ranged between 90% and 100% initially, then decreased with time until reaching approximate values of 80% to 85%. The loss of humidity was higher in magnitude and rate near the top surface of the bridge deck compared to the middle and bottom of the slab.

A 3D finite element model (FEM) was developed to predict the top and bottom structural strain values in the concrete deck that can be developed due to the weight of the bridge. A typical 12 in. (305 mm) mesh element was used for the FEM of the bridge deck, girders, and concrete diaphragm. The applied loads were limited to the self-weight plus the weight of the concrete bridge barrier on each side of the bridge. The modeling was conducted for the bridge deck at three different ages of 3, 56, and 260 days with the corresponding material properties that varied with time. The estimated strain values were compared to those recorded by the in-situ sensors in the longitudinal and transverse directions.

In the longitudinal direction, the stresses were shown to reach the maximum positive values at the points of contact of the girder with the concrete diaphragm. The values decreased gradually along the length of the bridge to reach the maximum negative values approximately at the mid-span of the bridge deck. In the transverse direction, the tensile stresses were positive near the diaphragm given the fact that the slab is acting as a top flange for the diaphragm, because the slab was cast monolithically with the diaphragm with a countoius steel reinforcing bar over the diaphragm. Away from the diaphragm the stresses were positive above the girders

and negative in between adjacent girders. The area under consideration, where the towers are located, was in complete tension in the longitudinal and transverse directions. The highest tensile strain values reached 2100 micro-strain at the intersection of the intermediate bent with one of the pre-cast concrete girders.

A strain model was proposed to evaluate the strain data collected from the embedded sensors. The model represents the total strain as a summation of strains due to thermal deformation, drying and autogenous shrinkage, and structural deformation. The model was used to evaluate strains and estimate values of the concrete shrinkage during the first 30-36 hours, which corresponded to the time of demolding of the shrinkage samples. The load distribution factor, defined as the ratio between the portion of the load carried out by the concrete slab to the total load carried out by the slab and stay-in-place corrugated sheet formwork as well as the supporting girders, was estimated from the proposed strain model. Findings indicated that the load distribution factor increased with concrete age reaching a value of 0.98 at 260 days. The concrete shrinkage during the first 30-36 hours was then estimated to be 75 micro-strain.

A fiber-reinforced super-workable concrete (FR-SWC) made with 0.5% micro-macro steel fibers and 5% CaO-based expansive agent was selected for the new deck slab reconstruction of Bridge A8509. The selected FR-SWC had a targeted slump flow of 20 in. at the casting location. Multiple trial batches were performed, in collaboration with the concrete supplier, to adjust the mixture composition to meet the targeted performance criteria. This was followed up by casting the fibrous concrete in a mock-up slab measuring 10×10 ft that was prepared to simulate the tight rebar and the roadway crown slope in the transverse direction. The results indicated the necessity to lower the concrete slump from the intended value for FR-

SWC to hold the 2% crown slope of the bridge deck in the transverse direction. The final mixture that was selected following the trial batches and mock-up placement had a slump consistency of 8 ± 2 in. (FRC). Six sensor towers were installed in the slab within 18 ft to the East and West sides of the intermediate bent to monitor in-situ properties of the concrete. Each tower had three humidity sensors, three thermocouples, and 12 concrete strain gauges. The slump values varied between 6 and 10 in. The fresh air volume ranged from 4.4% to 5.8%, and the concrete temperature ranged from 85 to 97 °F. At 56 days, the compressive strength ranged from 7,020 to 8,360 psi and had a mean value of 7,770 psi. Data up to 260 days are reported at the time of the preparation of this report. The in-situ concrete temperature was shown to increase around 45 °F during the first day, reaching a maximal temperature of 140 °F. The temperature then dropped to ambient temperature of approximately 95 °F during the second day. It then varied on a daily basis with the ambient temperature. The relative humidity of concrete ranged between 90% and 100% initially, then decreased with time until reaching approximate values of 80% to 85%. The loss of humidity was higher in magnitude and rate near the top surface of the bridge deck compared to the middle and bottom of the slab. A 3D finite element model (FEM) was developed to predict the top and bottom structural strain values in the concrete deck that can be developed due to the weight of the bridge. The estimated strain values were compared to those recorded by the in-situ sensors in the longitudinal and transverse directions. In the longitudinal direction, the stresses were shown to reach the maximum positive values at the points of contact of the girder with the concrete diaphragm. The values decreased gradually along the length of the bridge to reach the maximum negative values approximately at the mid-span of the bridge deck. The area under consideration, where the towers are located, was in complete tension in the longitudinal and

transverse directions. The highest tensile strain values reached 2100 micro-strain at the intersection of the intermediate bent with one of the pre-cast concrete girders. A strain model was proposed to evaluate the strain data collected from the embedded sensors. The model represents the total strain as a summation of strains due to thermal deformation, drying and autogenous shrinkage, and structural deformation. The model was used to evaluate strains and estimate values of the concrete shrinkage during the first 30-36 hours, which corresponded to the time of demolding of the shrinkage samples as well as the load distribution factor between the concrete slab and the steel corrugated sheet that varied with concrete age. Findings indicated that the load distribution factor increased with concrete age reaching a value of 0.98 at 260 days. The concrete shrinkage during the first 30-36 hours was then estimated to be 75 micro-strain.

A life cycle cost analysis (LCCA) was performed to estimate the life cycle cost (LCC) savings of using the FRC in bridge deck compared to regular bridge deck cast using conventional vibrated concrete (CVC). In addition to the Taos Bridge (Bridge 1), two reference bridges were considered in this analysis. The first reference bridge (Bridge 2) is located on Route 13 over the Log Creek near Kingston, MO. The bridge desk was cast using CVC. The bridge has two spans measuring 120 and 124 ft and has a width of 30 ft, which is geometrically similar to Bridge 1. Both bridges have one travel lane in each direction and are located in relatively low traffic areas. The analysis included traffic scenarios involving 668 and 3,387 ADT with truck traffics of 5% and 22%, respectively. The second reference bridge (Bridge 3) was considered at an area of much higher traffic volume (114,739 ADT and 1.55% truck traffic) in a different climate condition. The bridge is located on I-80 in New Jersey 0.7 miles

east of the Passaic River and is used as benchmark for LCCA studies in high traffic areas. The bridge deck was constructed using CVC.

The LCCA indicated that the use of FRC can provide cost savings for both user and social costs for the low and high traffic volume scenarios. It should be noted that although the percentage of cost savings is high in the case of the low volume scenario, the absolute values of the costs are actually small because of the low traffic volume (e.g., 668 ADT). When calculating the total LCC by summing up the agency, user, and social costs, the use of FRC was shown to provide a cost saving of up to 55% for the high traffic volume scenario.

Keywords: Bridge deck, crack resistance, embedded strain gauges, fiber-reinforced concrete, finite element modeling, flexural behavior, expansive agent analysis, macro fibers, micro fibers, super-workable concrete.

TABLE OF CONTENTS

LIST OF FIGURES

LIST OF TABLES

1   INTRODUCTION

This report presents the results of a field implementation involving the use of high-performance concrete with adopted rheology for the new slab deck of a bridge near Taos, Missouri. The two-span girder type bridge consists of four girders with span lengths measuring approximately 126 ft (38.4 m) and 115 ft (35.05 m) in length. The width of the bridge is 30 ft. The end bents and intermediate bent axes were skewed at 15 degrees to the axes of the girders, as shown in Figure 1. The FRC was developed as a part of a comprehensive research project undertaken to develop fiber-reinforced self-consolidating concrete (FR-SCC) for repair applications and fiber-reinforced super-workable concrete (FR-SWC) for infrastructure construction [1]. A FR-SWC made with 0.5% micro-macro steel fibers and 5% CaO-based expansive agent (EA) that can develop high tensile strength, low shrinkage, and high resistance to cracking was selected for the new deck slab of Bridge A8509 over Route 50 near Taos, Missouri, hereafter referred to as the Taos Bridge. Although the concrete was intended for construction of bridge substructure elements, a decision was made to use it for the new deck slab work given the anticipated high tensile stresses in the bridge deck at the intermediate bent and the relatively high concentration of steel reinforcement necessitating the use of a highly flowable fibrous mixture. A highly flowable fiber-reinforced concrete (FRC) was developed as a part of a comprehensive research project undertaken with the Missouri Department of Transportation (MoDOT) and the RE-CAST (Research on Concrete Applications for Sustainable Transportation) Tier-1 University Transportation Center.

Figure 1. Taos bridge elevation and plan

The project included the development of fiber-reinforced self-consolidating concrete (FR-SCC) for repair applications and fiber-reinforced super-workable concrete (FR-SWC) for infrastructure construction [1]. The FR-SWC made with 0.5% micro-macro steel fibers. A CaO-based expansive agent (EA) was added at a dosage of 5% of total binders. The purpose of using EA with fibers was to develop high tensile strength, low shrinkage, and high resistance to cracking. Although FR-SWC was developed originally for construction of bridge substructure elements, a decision was made to use it for casting of the new bridge deck. The spacing of the top and bottom reinforcement bars in the longitudinal direction was 7.5 and 5 in., respectively, and 6 and 8 in. in the transverse direction.

1.1 Project Objective

This report summarizes the results of an implementation project involving the use of a high-performance highly flowable FRC for the new deck slab of the Taos Bridge. The report discussed the properties of the concrete mixture used in the construction project, the in-situ properties of the concrete collected over 260 days, and the results of a detailed finite element modeling carried out to evaluate in-situ performance of the bridge deck. The reported study consisted of 10 tasks, as described below.

Task 1: Development of job special provisions

In collaboration with the MoDOT Bridge Division, a job special provisions document regarding the production and casting of the intended FR-SWC for the new deck slab of the Taos Bridge was produced. The document was developed to provide material characteristics, fresh and hardened properties, and develop a proven mixture composition for the FR-SWC.

Task 2: Trial batches

Trial batches were conducted in collaboration with the ready-mix concrete producer responsible for providing concrete to the job site. Key fresh and hardened concrete properties were determined using the intended constituent materials and chemical admixture. The performance of the concrete was compared to that of the proposed FR-SWC that was developed by the research team for the construction of bridge sub-elements [1]. Trial batches necessitated the modification of the proposed mixture to satisfy specific constructability constrains involving a 2% transverse crown slope for the bridge.

Task 3: Mock-up placement

A mock-up placement was carried out to verify the workability and finishability of the modified FRC and to evaluate its ability to hold the 2% crown slope.

Task 4: Instrumentation

A comprehensive program involving 108 sensors was undertaken to evaluate in-situ concrete properties. The sensors were employed to determine concrete temperature, relative humidity, and strain variations at different locations of the bridge deck.

Task 5: Sampled concrete properties

This task involved taking concrete samples from seven ready-mix trucks out of the 40 truck deliveries used for the bridge deck construction. Concrete was tested to determine workability, compressive strength, splitting tensile strength, flexural strength, elastic modulus, and drying shrinkage.

Task 6: Data acquisition and in-situ performance

Data were collected on a weekly basis from six different locations on the bridge deck using a data acquisition system. Sensors were positioned near the top, middle, and bottom of the 8.5 in.-thick bridge deck slab in the longitudinal and transverse directions.

Task 7: Finite element analysis

A 3D finite element model (FEM) was developed to estimate strains in the concrete deck due to the bridge's own weight. The FEM included the FRC that was used for the deck and diaphragm, as well as the pre-cast concrete used for the girders.

Task 8: Strain analysis

Thermal deformations of the concrete slab, concrete shrinkage, and structural deformation were considered in the strain analysis. The analysis was used to estimate concrete shrinkage during before the demolding of the shrinkage prisms and the load distribution factor that reflects the portion of the load carried out by the concrete slab.

Task 9: Field inspection

A field inspection was carried out to evaluate cracking and deterioration of the bridge deck.

Task 10: Life cycle and cost analysis

A life cycle cost analysis (LCCA) was conducted to quantify life cycle cost savings that may result from using FRC in the bridge deck construction.

2   JOB SPECIAL PROVISIONS

In collaboration with the MoDOT Bridge Division, a job special provisions document involving the production and casting of the intended FR-SWC for the new deck slab of the Taos Bridge was produced. The document was developed to provide material characteristics, fresh and hardened properties, and develop a proven mixture composition for the FR-SWC. Table 1 summarizes the mixture proportioning of the proposed concrete. A combination of micro and macro steel fibers was proposed to produce the FR-SWC at a fiber volume of 0.5% (67 lb/yd^3). A binary cement made with 70% Type I/II portland cement and 30% Class C fly ash was proposed. A Type G CaO-based expansive agent (EA) corresponding to 5% of the total binder mass was specified to induce an initial expansion and compensate for some of the shrinkage of the concrete. The targeted water-to-cementitious materials ratio (w/cm) was 0.42 to enhance the durability of the concrete.

Table 1. Proposed mixture proportioning of FR-SWC

Type I/II Cement (pcy) [kg/m^3]	Class C fly ash (pcy) [kg/m^3]	Type G EA (pcy) [kg/m^3]	Water (pcy) [l/m^3]	Coarse agg. (NMSA ½ in.) (pcy) [kg/m^3]	Sand (pcy) [kg/m^3]	Fibers (pcy) [kg/m^3] Macro 30 mm (1.2 in.)	Fibers (pcy) [kg/m^3] Micro 13 mm (0.5 in.)	VMA (fl oz/yd^3) [l/m^3]	HRWR (fl oz/yd^3) [L/m^3]	AEA (fl oz/yd^3) [ml/m^3]
430 [255]	185 [110]	32 [19]	265 [157]	1,268 [752]	1,552 [921]	54 [24.5]	13 [6]	60 [2.3]	98 [3.8]	1.1 [42]

Continuously graded crushed limestone aggregate with a nominal maximum size of aggregate (NMSA) of 0.5 in. was used. The specified high range water reducing admixture (HRWRA), air-entraining admixture (AEA), viscosity-modifying admixture (VMA), and EA were the same as those of the presented FR-SWC in Reference 1. This was in exception for the dosage of the EA that was increased from 4% to 5% to further reduce drying shrinkage.

Table 2 summarizes the performance-based specifications for the recommended FR-SWC mixture. The concrete is expected to develop an initial slump flow ranging of 20 to 23 in., an air content of 6% to 9%, and high static stability with a visual stability index (VSI) of 0. The difference between the slump flow diameter and that of the modified J-Ring test should be less than 2 in. in order to ensure high passing ability. After 7 days of moist curing, the concrete should have a maximum drying shrinkage of 450 µstrain after 120 days of drying.

Table 2. Characteristics of proposed FR-SWC mixture

Fresh Properties

Time (minute)	20	40	60	80
Slump flow (in.) [mm] (ASTM C1611)	22 [560]	21.5 [545]	19.5 [495]	17.5 [445]
VSI (ASTM C1611)	0	0	0	0
T-40 (sec)	1.5	2	3	5.5
Mod. J-Ring diameter (in.) [mm]	21 [535]	21 [535]	19 [485]	-
Air content (%) (ASTM C231)	8	7	7	6.5
Unit weight (pcf) [kg/m³] (ASTM C138)	142 [2270]	142 [2270]	142 [2270]	142 [2270]

Hardened Properties

Age (days)	3	7	28	56
Compressive strength (psi) [MPa] (ASTM C39)	35,00 [24.5]	5,000 [34.5]	6,400 [45]	7,250 [50]
Flexural strength (psi) [MPa] (ASTM C78)	-	-	785 [5.5]	840 [5.9]
Drying shrinkage, 7 days of moist-curing (ASTM C157)	450 µstrain after 120 days	450 µstrain after 120 days	450 µstrain after 120 days	450 µstrain after 120 days
Restrained shrinkage (ASTM C1581)	Low potential for cracking	Low potential for cracking	Low potential for cracking	Low potential for cracking

After discussion between the research team, MoDOT Bridge Division, MoDOT Research Division, the contractor, and the concrete supplier, a decision was made to limit the concrete slump to 10 in. instead of a slump flow of 22 in. in order to prevent any possible flow of the concrete over the 2% crown of the bridge deck.

3   TRIAL BATCHES

Between May 11 and 18, 2017, five trial batches were prepared with the concrete supplier to re-produce the targeted mixture using the locally available materials. All mixtures had the same cement and fly ash as recommended mixture in Table 1 (430 pcy of cement Type I/II and 185 pcy of Class C fly ash) and had a constant dosage of AEA of 3.3 fl oz/yd^3 to secure an initial air volume of 5.5% to 7%. The EA dosage was kept constant at 5% binder mass. The HRWR dosage was adjusted to control the slump consistency.

Table 3. Mixture proportioning and fresh properties off the trial batches

Mixture no.	Adjusted w/cm	HRWR (fl oz/yd^3)	Time of test (min.)	Slump (in.)	Slump flow diameter (in.)	Mod. J-Ring (in.)	Air content (%)
1	0.46*	120	40	7.5	-	-	6.4
1	0.46*	120	60	7	-	-	6.2
2	0.46*	140	80	9	15	14.5	6.8
3	0.46*	160	100	10	16.5	15.5	6
4	0.46*	200	120	-	20	19	5.5
4	0.46*	200	165	10	16	16	5.5
5	0.42	120	20	9	-	-	6.5
5	0.42	120	40	8	-	-	6.3
5	0.42	120	80	7.5	-	-	6.2
5	0.42	120	80	6	-	-	6

* Sand moisture was not determined correctly resulting in higher w/cm than the targeted value of 0.42.

Table 3 presents a summary of the trial batches. Mixture 5 with an initial slump of 9 and 8 in. after 20 and 40 minutes, respectively, was selected for the mock-up placement.

4   MOCK-UP PLACEMENT

A 10 x 10 ft mock-up slab with different densities of reinforcing bars was cast a week before the anticipated new deck slab of the bridge. As shown in Figure 2, the reinforcing bars' densities representing different areas of the bridge deck were included to evaluate the workability and finishability of the proposed FRC mixture. Table 4 compares the concrete performance obtained during the trial batches and later during the mock-up test.
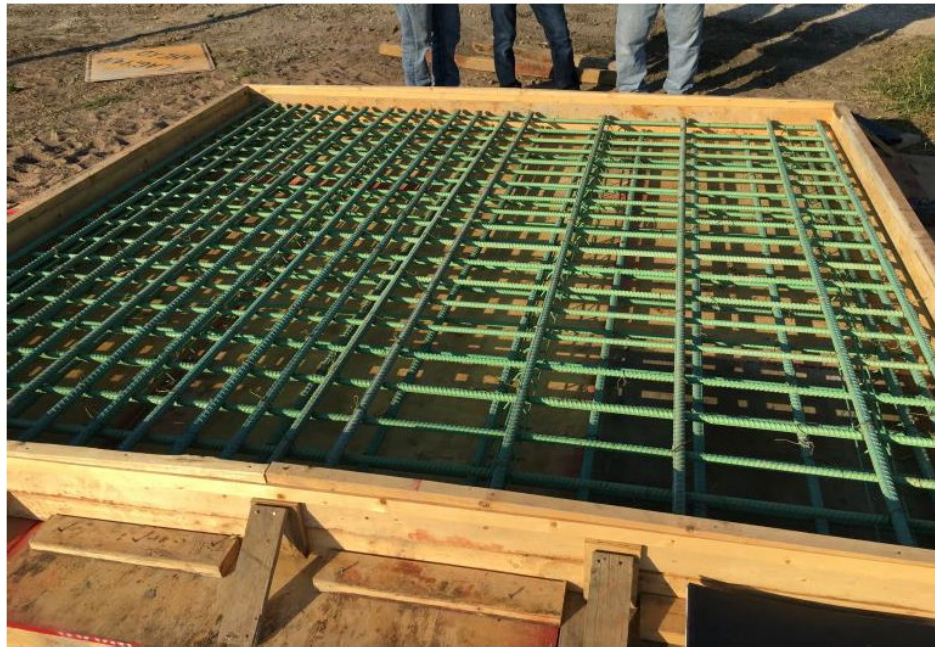
Figure 2. Mock-up slab placement with different top rebar densities of 5 x 6 in. and 10 x 6 in. that correspond to different locations along the bridge desk

Table 4. Properties of concrete cast for mock-up test vs. successful trial mixture

Fresh property	Trial batch	Mock-up
Concrete temperature (°F)	83	91
Initial slump (in.)	8.50	Not available
Slump at 40 min (in.) corresponding to time of concrete delivery	8.00	8.75 - directly from truck
Slump at 60 min (in.)	7.50	8.00 - end of pumpline
Slump at 80 min (in.)	6.00	4.50 - wheel barrow
Air volume at 50 min (in.)	6.25	5.50 - end of pump hose
Air volume at 60 min (in.)	6.25	4.75 - end of pump hose
Air volume at 80 min (in.)	6.00	4.5 - wheel barrow

Based on the results of the mock-up testing, the following observations and recommendations can be made:

➢ The full anticipated dosage of the HRWRA was added upon arrival of the concrete truck to site. The concrete slump at 40 min was 8.75 in. when sampled from the back of the truck and 8 in. at the end of pumpline.

➢ Given the high slump of the concrete, the concrete surface did not maintain its profile and exhibited some settlement. Therefore, recommendations were made to lower the HRWRA dosage in order to reduce the slump of the concrete after pumping to approximately 6 in.

➢ The initial concrete temperature measured off the truck was 91 °F. Such high temperature can lead to sharp loss of workability and anticipated difficulties in consolidation and finishing. It was recommended to use ice to replace some of the mixing water to reduce concrete temperature to mid-70s °F for the bridge deck placement.

➢ Rapid drying and tearing of surface was observed before the use of a finishing aid. The use of the finishing aid proved to be effective in finishing the concrete during the mock-up placement.

➢ A large internal vibrator was employed and was not kept immersed in the concrete for a long time to avoid segregation. It was recommended to use smaller vibrators (e.g., 1- 1.5 in. in diameter) and to keep it in the concrete for enough time to ensure proper consolidation without increasing the risk of segregation.

➢ Plastic shrinkage measures were recommended to mitigate the risk of plastic shrinkage. This includes fogging on the job site, casting concrete early morning or night, protect the surface from drying at all time, and the use of evaporation retarder.

➢ It was recommended to develop plans for the finishing of the concrete to ensure that the concrete surface can be adequately finished and decide on the actual need for the finishing aid.

➢ It was also recommended to consult the fiber manufacturer about best practices for casting and finishing of FRC.

5   INSTRUMENTATION

The bridge deck was instrumented with embedded strain gauges, relative humidity sensors, and thermocouples to monitor concrete strains, relative humidity, and temperature, respectively. Each of the six sets of the sensor towers had 18 sensors attached onto a plastic frame, as shown in Figure 3. Six concrete embedded strain gauges were placed on each tower, near the top, middle, and bottom sections of the concrete deck in both the longitudinal and transverse directions. Another set of six strain gauges were put directly adjacent to the reinforcing steel bars in order to determine the strains of the concrete near the reinforcing bars. Three of these strain gauges were placed in the longitudinal direction and another three in the transverse direction. Three relative humidity sensors were added to each tower near the top, middle, and bottom levels. Three thermocouples were also used at each tower near the top, middle, and bottom levels. Six sensor towers were positioned at different locations of the concrete deck around the intermediate bent, where high tensile stresses are expected, as shown in Figure 4.
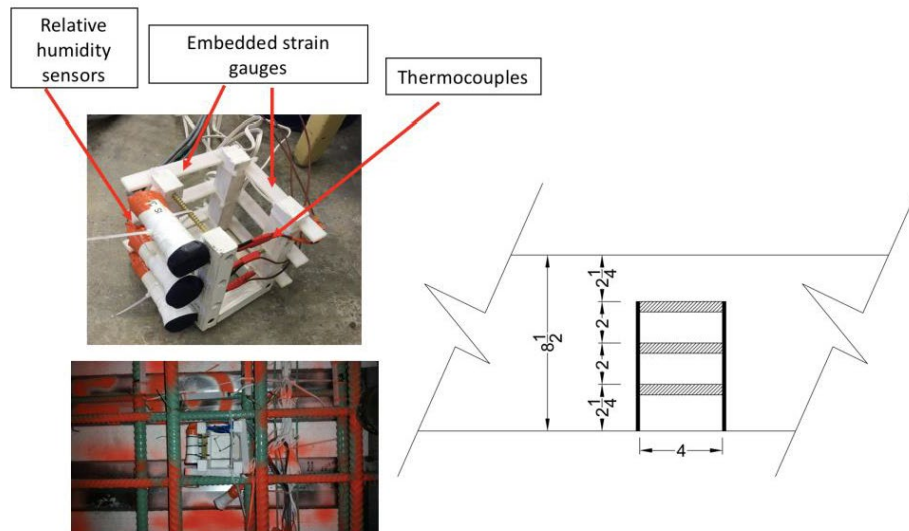
Figure 3. Instrumentation and dimensions of the sensor tower
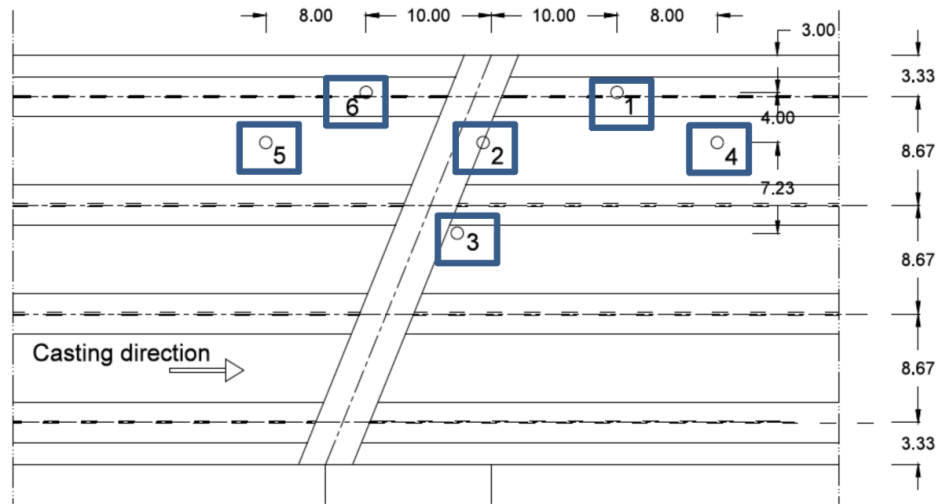
Figure 4. Sensor tower locations around the intermediate bent

In total, 108 wires were used to connect sensors. The sensors were connected into 108 channels of a data acquisition system (DAS). In order to identify the wires and hook each wire to the right channel, a codification was implemented. Each set of sensor wires was labeled with different color labels and a unique code for each label.

Table 5 shows the wire codification used to identify the sensor wires on one of the six towers. The wiring identifications for the other five sensor towers are provided in Appendix 1. The DAS was connected to a modem to transmit data remotely to Missouri S&T on a daily basis. A solar panel was used to provide the DAS with power, as shown in Figure 4.

Table 5. Wire identification

Gauge type, number, and direction	Labeling color	Labeling code	Length (ft)	Starting foot marker	Ending foot marker
Concrete 1 Long.	White	1-C-1	22	2234	2256
Concrete 2 Long.	White	1-C-2	22	2256	2278
Concrete 3 Long.	White	1-C-3	22	2278	2300
Concrete 4 Trans.	Yellow	1-C-4	22	2300	2322
Concrete 5 Trans.	Yellow	1-C-5	22	2322	2344
Concrete 6 Trans.	Yellow	1-C-6	22	2344	2366
Rebar 1 Long.	Blue	1-R-1	24	2366	2390
Rebar 2 Long.	Blue	1-R-2	24	2390	2414
Rebar 3 Long.	Blue	1-R-3	24	2414	2438
Rebar 4 Trans.	Red	1-R-4	24	2438	2462
Rebar 5 Trans.	Red	1-R-5	24	2462	2486
Rebar 6 Trans.	Red	1-R-6	24	2486	2510
Humidity 1	Green	1-H-1	22	2510	2532
Humidity 2	Green	1-H-2	22	2532	2554
Humidity 3	Green	1-H-3	22	2554	2576
Thermocouple 1	Orange	1-T-1	22	-	-
Thermocouple 2	Orange	1-T-2	22	-	-
Thermocouple 3	Orange	1-T-3	22	-	-

The instrumentation of the bridge deck was performed after the completion of the placement of the top and bottom steel reinforcing bars on the bridge deck. This was done to minimize the risk of damage to the sensors. A limited number of sensors was damaged during the concrete placement operations.

Figure 5. Data acquisition system and solar cell positioned at the intermediate bent

6   CONCRETE PROPERTIES

6.1   Concrete placement

The placement of the FRC was carried out between approximately midnight and 7 am on July 26, 2017. In total, of 330 yd^3 of FRC were cast. The concrete was successfully placed using two pumps located on the East and West sides of the bridge. In total, 40 deliveries of concrete batched at volumes of 8.25 yd^3 were used for the mixing and delivery of the concrete. Given the high ambient temperature, ice was used as partial replacement of the mixing water starting with the 12th truck delivery, as noted in Table 6.

The sampling of the concrete for workability and compressive strength testing was done for truck deliveries 2, 7, 12, 25, 21, 33, and 40. All sampling was made at the end of pumpline. Truck deliveries 21, 33, 37, and 40 were also sampled to evaluate splitting tensile strength, flexural strength, elastic modulus, and drying shrinkage. Unfortunately, the samples from Truck #37 were damaged by some construction activities before the recovery of the test samples. The cylindrical 4 × 8 in. samples were prepared to determine compressive and splitting tensile strengths and modulus of elasticity and were cast in two lifts and subjected to consolidation using 3/8-in. diameter rods. Prismatic samples measuring 3 × 3 × 16 in. were used to evaluate flexural strength, and 3 × 3 × 11.25 in. prisms were used to determine drying shrinkage. All prismatic samples were cast in two lifts and consolidating using 3/8-in. steel rods.

The samples were stored under wet burlap and plastic sheets and were then transported under wet conditions to the Advanced Construction Materials Laboratory at Missouri S&T. The samples were de-molded at 30-36 hour of age, depending on the sampled concrete delivery, then subjected to moist curing in lime-saturated water. The samples used to determine

mechanical properties were maintained under saturated conditions until the time of testing. The prisms used for drying shrinkage were then stored at 50% ± 4% relative humidity at 72 ± 2 °F. Figure 6 shows photographs of the concrete pumping, placement, sampling, and finishing activities.

6.2   Fresh concrete properties

Table 6 summarizes the fresh properties for samples taken from the seven sampled trucks. For Truck #2, half of HRWRA was added at the batching plant with the other half divided into two parts for addition as needed on site. Starting at Truck #12, ice was used from ice bags added to the back of the ready-mix trucks on the job site. As indicated in Table 6, the sampled trucks had 24 lb/yd^3 of ice added at the job site. The equivalent water was held back at the batching plant to maintain the same w/cm. The slump consistency of the seven sampled trucks determined after pumping ranged from 6 to 10 in., the air volume ranged from 4.4% to 5.8%, and the concrete temperature ranged from 85 to 97 °F.

6.3   Hardened concrete properties

Compressive strength at 28 and 56 days was determined for samples taken from seven trucks. Samples taken from Trucks # 21, 33, and 40 were further tested for splitting tensile strength, flexural strength, elastic modulus, and drying shrinkage. Three samples were used for compressive strength and splitting tensile strength, as shown in Table 7. The mean compressive strength values ranged from 5,780 to 6,980 psi at 28 days with an overall mean value of 6,450 psi. These values ranged from 7,020 to 8,360 psi at 56 days with an overall average value of 7,770 psi.
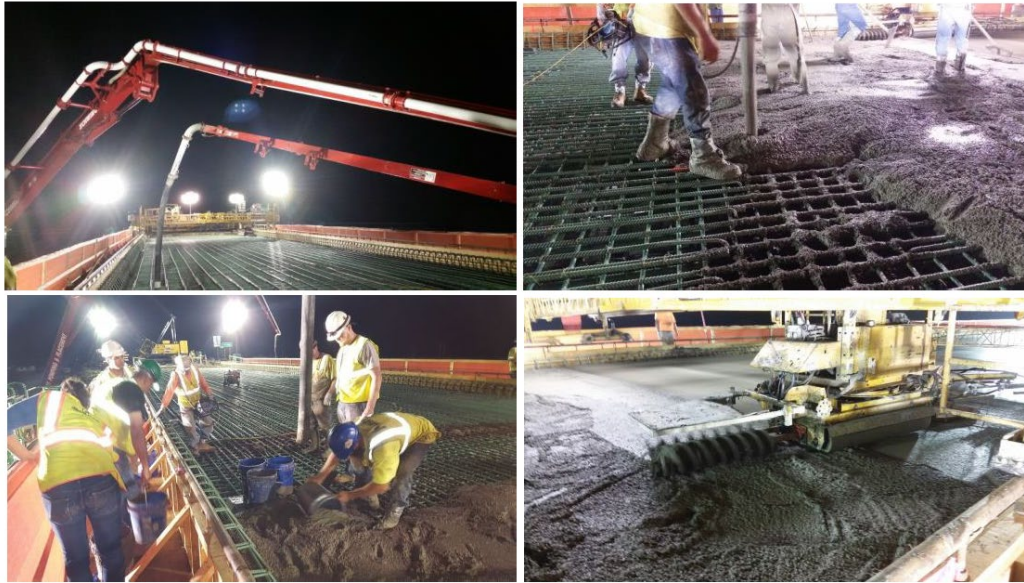
Figure 6. Concrete pumping, placement, sampling, and finishing

Table 6. Fresh properties of concrete samples taken from different truck deliveries

Truck no.	HRWR added on site (% of total anticipated dosage)	Ice added on site (pcy)	Time of sampling at end of pump	Ambient / concrete temperature	Slump Time	Slump in.	Air volume Time	Air volume %	Unit weigh (pcf)
2	75% (3.45 L/m^3)	0	0:55	82.8 / 96.8 ^{o}F (28 / 36 ^{o}C)	1:08	6.00	1:10	4.4	147.9
7	100% (4.6 L/m^3)	0	1:50	80 / 90.5 ^{o}F (27 / 33 ^{o}C)	2:00	8.75	2:02	3.8	146.9
12	70% (3.2 L/m^3)	24	3:00	73.4 / 86.5 ^{o}F (23 / 30 ^{o}C)	3:10	10.00	3:10	5.5	142.4
25	63% (2.9 L/m^3)	24	4:50	73 / 87.1 ^{o}F (23 / 31 ^{o}C)	5:15	6.00	5:20	5.8	144.0
21	75% (3.45 L/m^3)	24	3:15	75.7 / 86.9 ^{o}F (24 / 31 ^{o}C)	3:25	6.25	4:30	5.2	144.4
33	75% (3.45 L/m^3)	24	5:50	72.3 / 84.7 ^{o}F (22 / 29 ^{o}C)	5:55	8.50	6:02	5.4	144.0
40	75% (3.45 L/m^3)	24	6:30	75.7 / 88.9 ^{o}F (24 / 32 ^{o}C)	6:40	8.50	6:45	5.2	143.3

The mean splitting tensile strength values ranged from 780 to 1,050 psi at 28 days with an overall mean value of 940 psi. These values ranged from 1,130 to 890 psi at 56 days with an overall average value of 1,010 psi. Four samples were taken from each truck to determine the 56-day flexural strength. The 56-day flexural strength ranged from 770 to 910 psi with an overall mean value of 845 psi.

Samples prepared for testing the elastic modulus were tested after 3 and 56 days. The average 3- and 56-day elastic modulus values were 3,660 and 3,855 ksi, respectively. Two samples were taken from each truck for drying shrinkage testing. Figure 7 shows the drying shrinkage results for concrete sampled from three trucks. The initial expansion reached a peak value after 7 days, corresponding to the end of moist curing, with an average expansion of 125 micro-strain. The concrete exhibited shrinkage thereafter. The average shrinkage values of all tested samples after 56 and 260 days were limited to 185 and 320 micro-strain, respectively.

Table 7. Mechanical properties and drying shrinkage

Truck no.	f'_c (psi) (C.O.V., %) 28 d	f'_c (psi) (C.O.V., %) 56 d	f_t (psi) (C.O.V., %) 28 d	f_t (psi) (C.O.V., %) 28 d	Flexural strength (psi) 3 d	Flexural strength (psi) 56 d	E-modulus (ksi) 3 d	E-modulus (ksi) 56 d	Drying shrinkage (micro-strain) 28 d
2	7,080 6,810 7,050 **6,980** **(2.1)**	8,530 8,190 - **8,360**	X	X	X	X	X	X	X
7	6,610 6,570 6,320 **6,500** **(2.4)**	7,550 8,110 - **7,830**	X	X	X	X	X	X	X
12	5,420 5,370 6,240 **5,780** **(8.6)**	7,550 7,050 6,450 **7,020** **(7.8)**	X	X	X	X	X	X	X
25	6,990 6,690 6,980 **6,890** **(2.5)**	8,300 - **8,300**	X	X	X	X	X	X	X
21	6,770 6,710 6,860 **6,780** **(1.1)**	8,100 7,850 8,420 **8,120** **(3.5)**	780 970 840 **860** **(11.3)**	960 890 990 **950** **(5.4)**	780 970 840 **860** **(11.3)**	780 770 810 830 **800** **(3.3)**	3,750 3,780 **3,765**	3,930 3,980 **3,955**	-600 -610 **-605**
33	6,120 6,570 6,280 **6,320** **(3.6)**	7,580 7,850 7,320 **7,580** **(3.5)**	1,050 1,040 890 **990 (9)**	1,130 1,100 970 **1,070** **(7.9)**	1,050 1,040 890 **990 (9)**	800 860 910 800 **840** **(5.6)**	3,690 3,720 **3,705**	3,870 3,920 **3,895**	-595 -585 **-580**
40	5,250* 6,210 6,170 **5,880** **(9.2)**	7,580 6,850 7,060 **7,160** **(5.2)**	1,060 1,020 920 **1,000** **(7.2)**	1,190 1,080 1,150 **1,140** **(4.9)**	1,060 1,020 920 **1,000** **(7.2)**	880 860 910 930 **900** **(3.6)**	3,570 3,450 **3,510**	3,690 3,740 **3,715**	-580 -610 **-495**

*sample may be damaged

Two 3.75 × 8 in. cores were taken from the mock-up slab to measure the coefficient of thermal expansion (CTE). The cores dimensions were not matching the standard CTE test (AASHTO 336-09). A customized test was performed using surface attached strain gauges and thermocouples attached to the cores surface and hooked to a data accusation system. The samples were submerged in water and were put in a temperature control chamber. The temperature was changed from approximately 72 °F to 126 °F then back to 72 °F. The average measured value of the CTE was 1.772×10^{-5} micro-strain/°F.
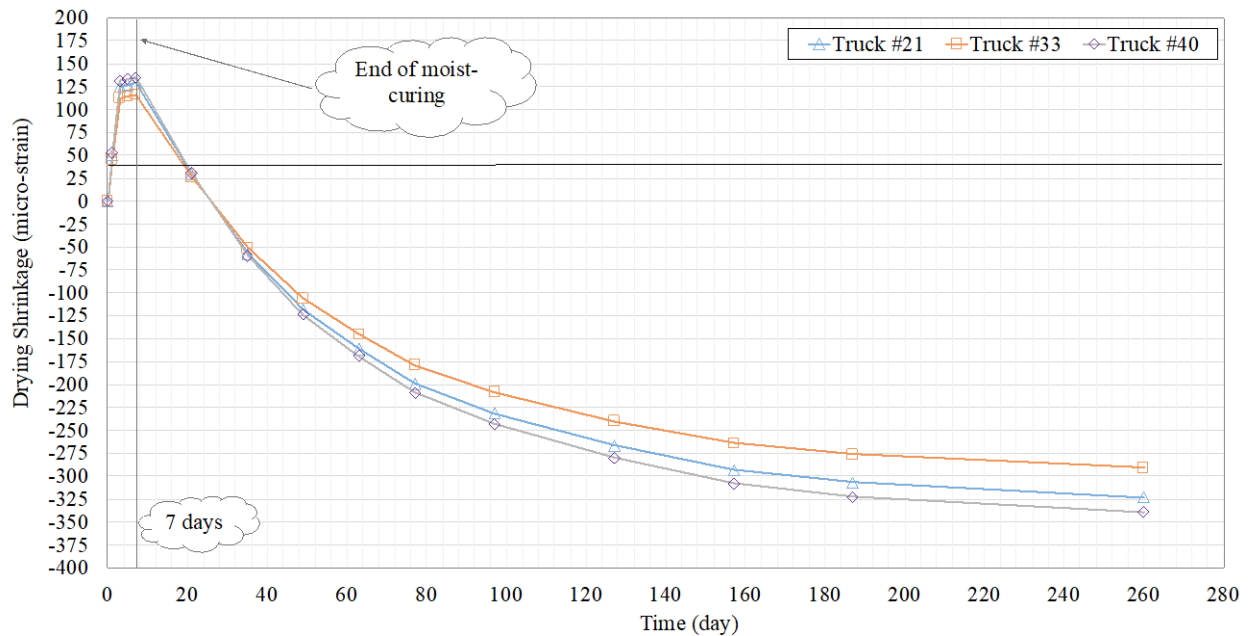
Figure 7. Drying shrinkage results from different results

7   IN-SITU DATA ACQUISITION

Figure 8 plots the variations of temperatures determined for the six towers. The data are provided for thermocouples near the upper, middle, and lower sections of the concrete deck (referred to here as Temp. 1, Temp. 2, and Temp. 3, respectively). The temperature was shown to increase by 45 ^{o}F at the first day to reach 140 ^{o}F and dropped to the ambient temperature of approximately 95 ^{o}F after one day and varied on daily basis thereafter.

Figure 9 shows the variations of concrete strain near the upper, middle, and lower sections of the concrete deck in the longitudinal and transverse directions. The strain is the summation of the structural strain due to self-weight of the concrete, strain due to the variations in the temperature, and strain due to shrinkage or expansion of the concrete material. The highest tensile strain of approximately to 2,100 micro-strain was recorded near the top of the bridge deck at the intersection of the intermediate bent with one of the pre-cast concrete girders.

Figure 10 shows the variations of the total strain in the concrete determined immediately adjacent to the steel reinforcement in the longitudinal and transverse directions. Sensors Long 1, Long 2, and Long 3 correspond to three embedded sensors located adjacent to three longitudinal top steel reinforcing bars close to sensor towers under consideration. Similarly, sensors Trans 1, Trans 2, and Trans 3 are three embedded sensors located adjacent to three transverse top steel reinforcing bars close to the sensor towers under consideration.
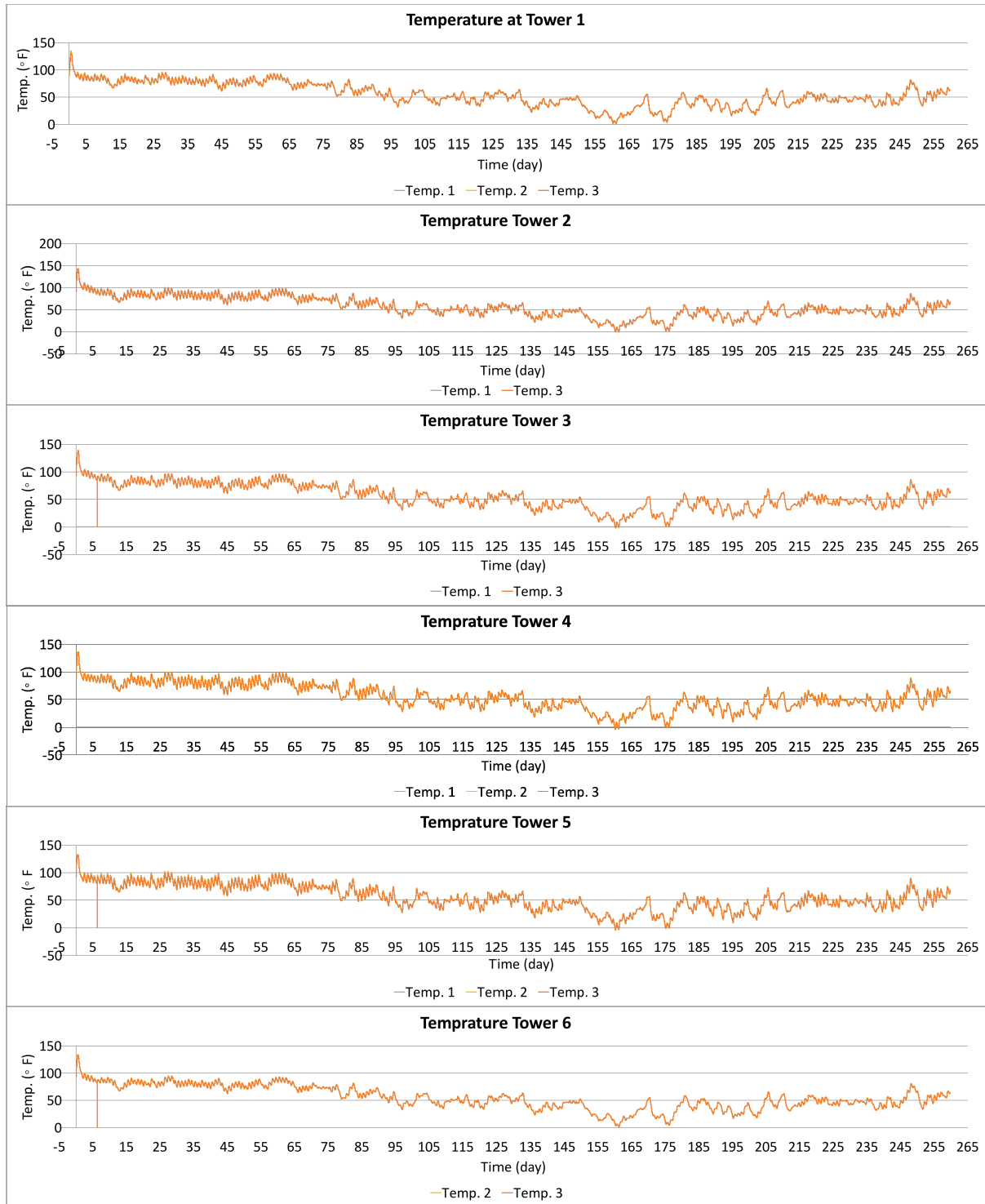
Figure 8. Temperature variations at upper, middle, and lower layers of concrete deck (1, 2, and 3, respectively) for the six sensor towers
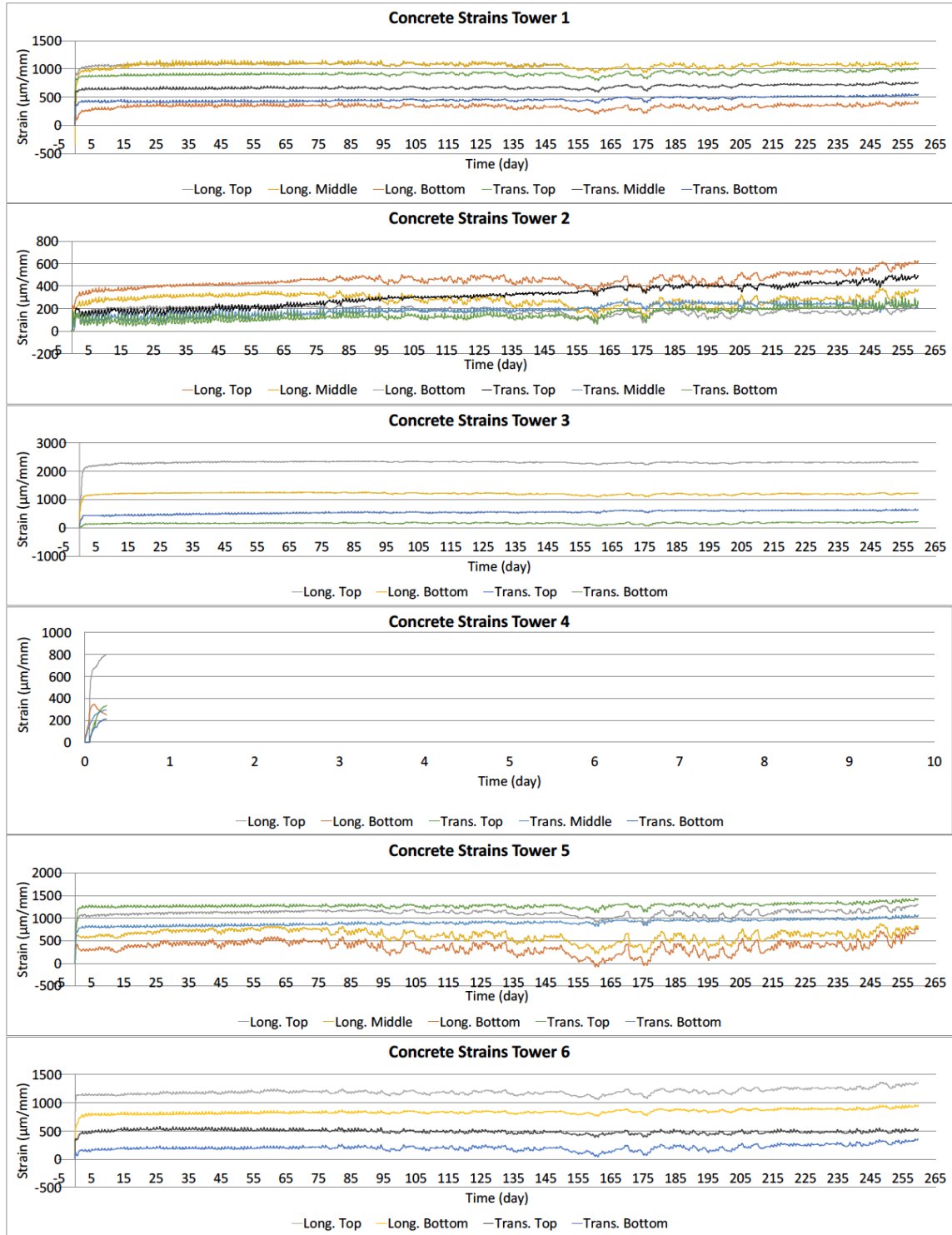
Figure 9. Variations of the concrete strain at upper, middle, and lower layers of concrete deck in the longitudinal and transverse directions for the six sensor towers
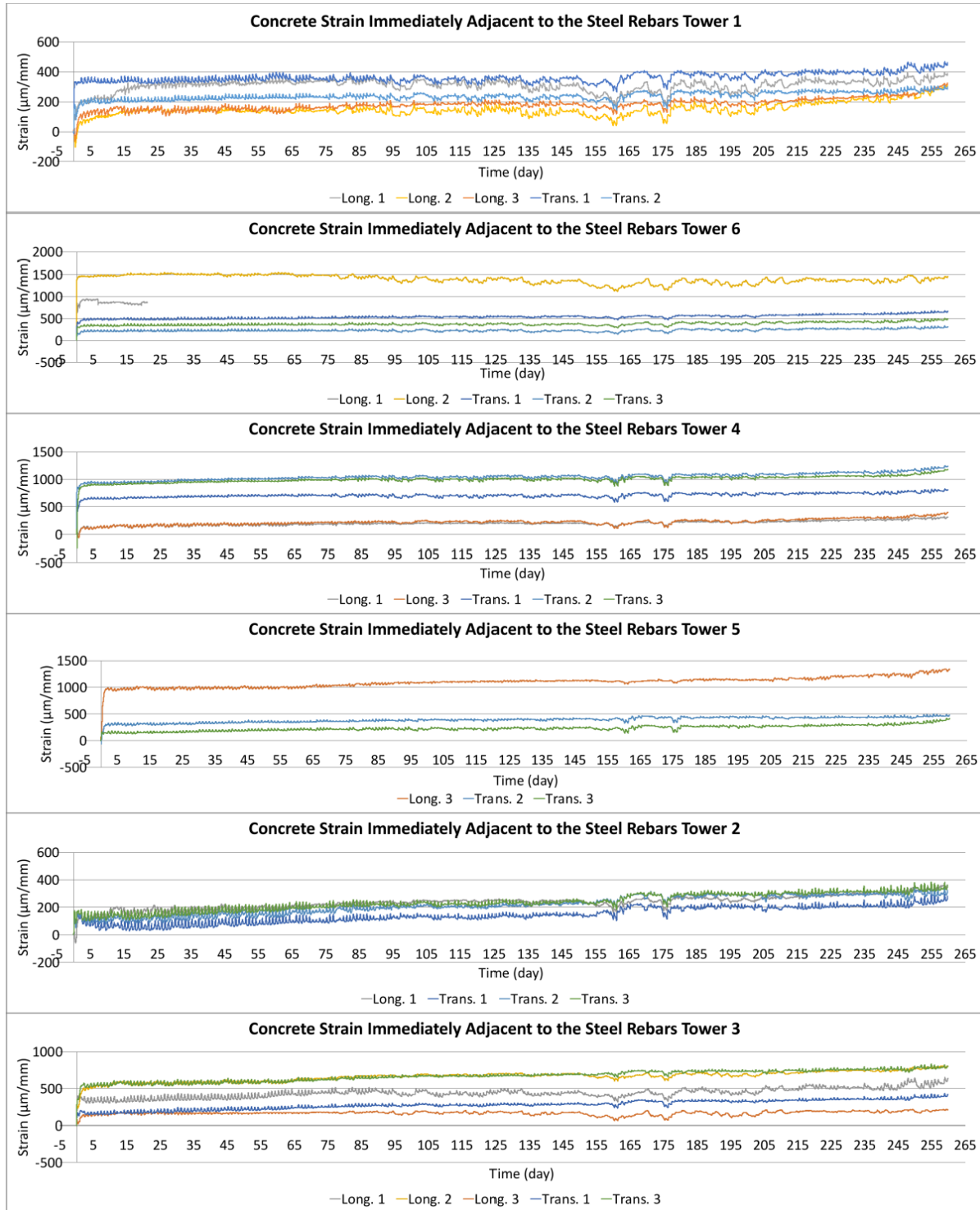
Figure 10. Variations of concrete strain determined adjacent to steel reinforcing bars in the longitudinal and transverse directions located at the six sensor towers

Figure 11 shows the variations of the relative humidity that ranged between 90% and 100%. The values then decreased with time to reach values of 82.5% ± 2.5%. The loss in relative humidity was sharper near the top of the bridge deck than that in the middle or the bottom sections.

The steady state relative humidity value at the top was approximately 80% compared to 85% and 82% at the middle and lower parts of the deck. The variations of relative humidity were minor beyond 60 ± 5 days, as indicated in Figure 11; the variations are therefore portrayed as straight lines. The in-situ data were collected up to 260 days at the time of preparation of this report. The sensors will continue to be monitored to update the results.
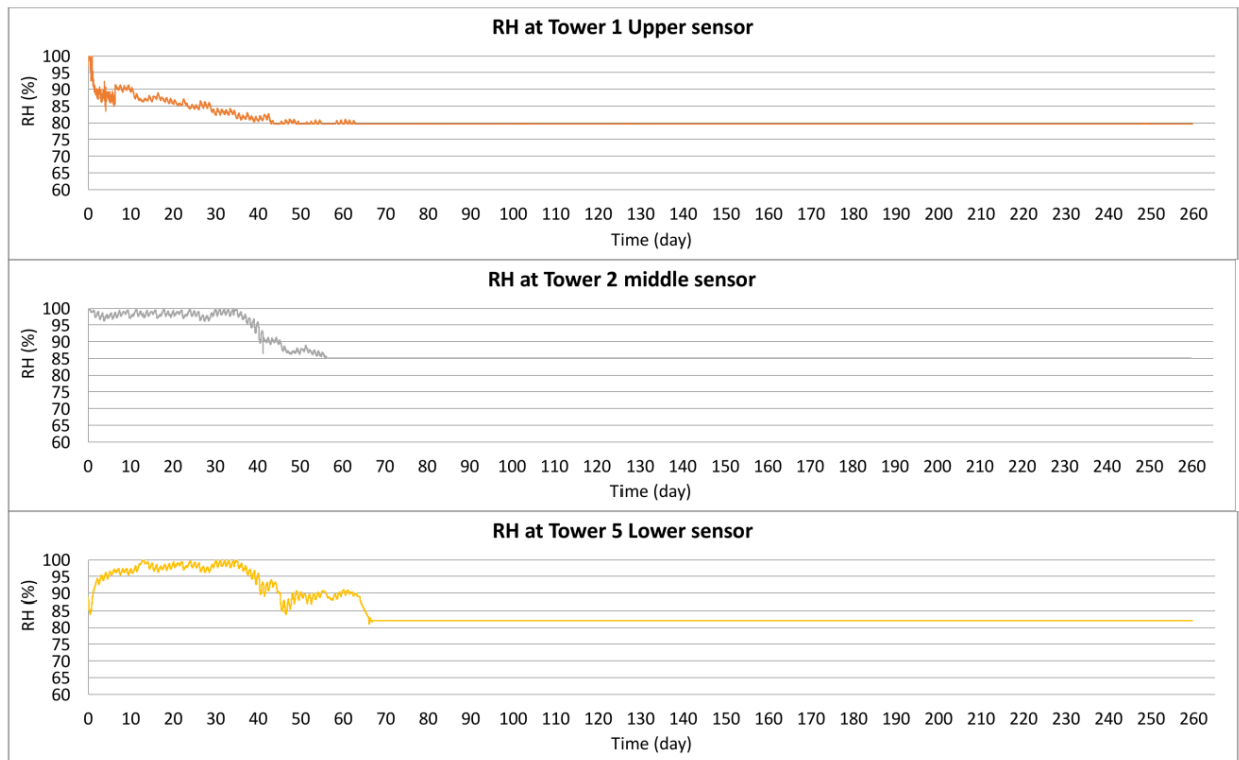
Figure 11. Variations of relative humidity of concrete at sensor towers 1, 2, and 5

8   FINITE ELEMENT MODELING

A 3D finite element model (FEM) was developed using SAP2000 to predict the top and bottom strains in the concrete deck due to the self-weight of the bridge in the longitudinal and transverse directions. As shown in Figure 12, two coordinate systems (X_1-Y_1 and X_2-Y_2) were used to model the bridge given the presence of the end bents and intermediate bent axes that are at a skew of 15 degrees to the axes of the girders. Only area elements were used to model this bridge. The bridge deck was divided into elements above the girders where the mesh thickness was equivilant to the slab thickness plus the upper flange thickness as well as elements between the girders with a thickness equivilant to the slab thickness. The bridge girders were simply supported. Two materials were defined: FRC used for modeling the concrete deck and diaphragm at the intermediate bent as well as the pre-cast concrete that was used for the bridge girders. The compressive strength and elastic modulus of the precast girders were taken as 8,000 psi and 5,000 ksi, respectively.

FEMs models were run at concrete ages of 3, 56, and 260 days where the modulus of elasticity values were 3,660, 3855, and 4100 ksi, respectively. A typical 12 in. mesh element was used for meshing the bridge, as shown in Figure 13. Loads included the self-weight of all modeled elements plus the weight of the concrete side bridge barrier that was applied as a line-load to the side-edges of the bridge. Figure 14 shows the deformed shape of the bridge.

3-D View

3-D View
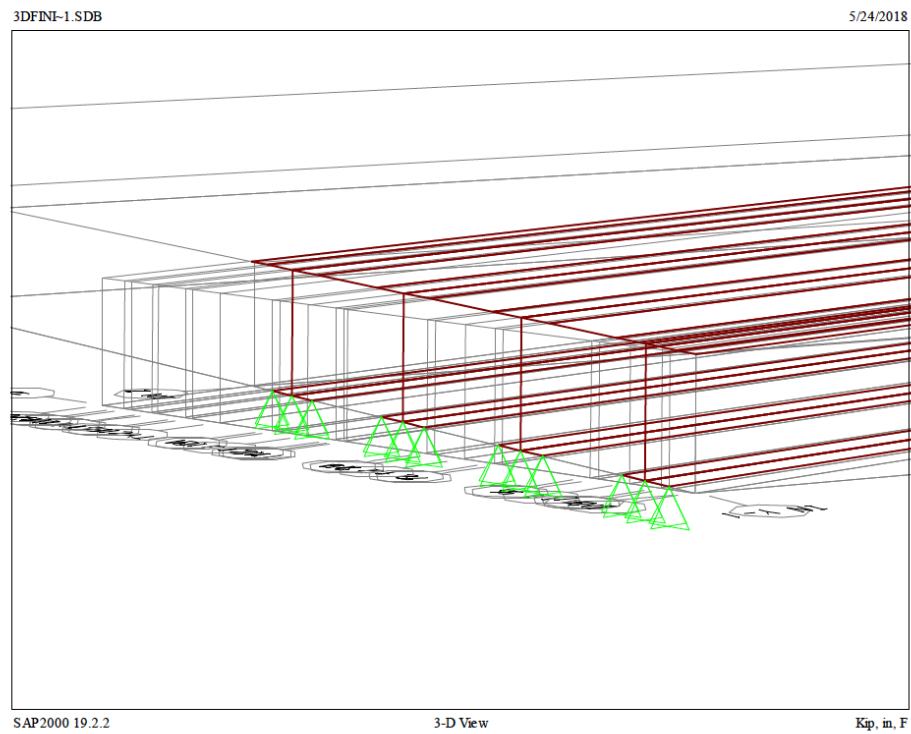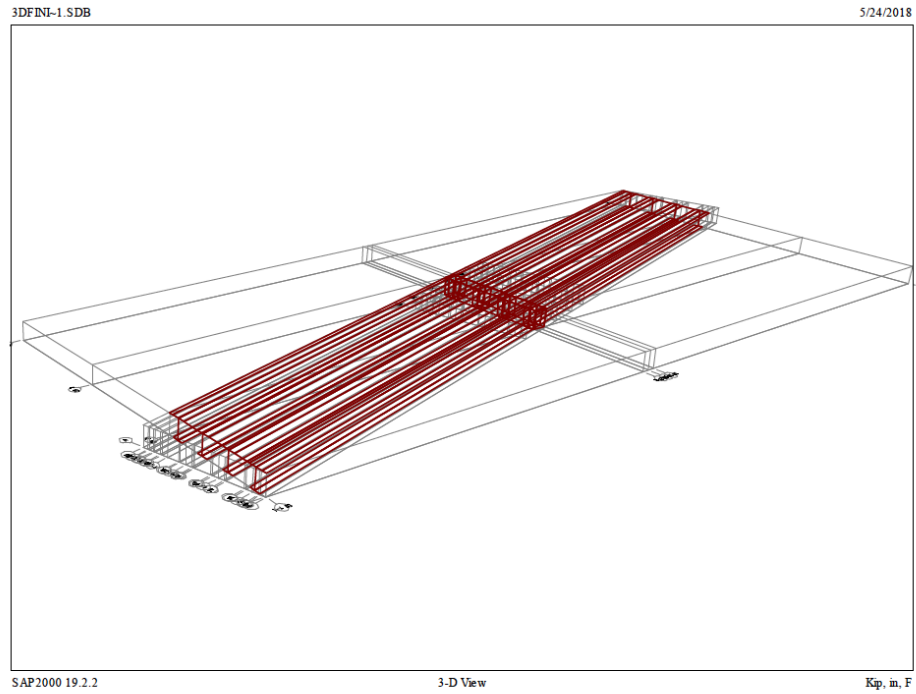
Figure 12. 3D finite element modeling of Taos Bridge
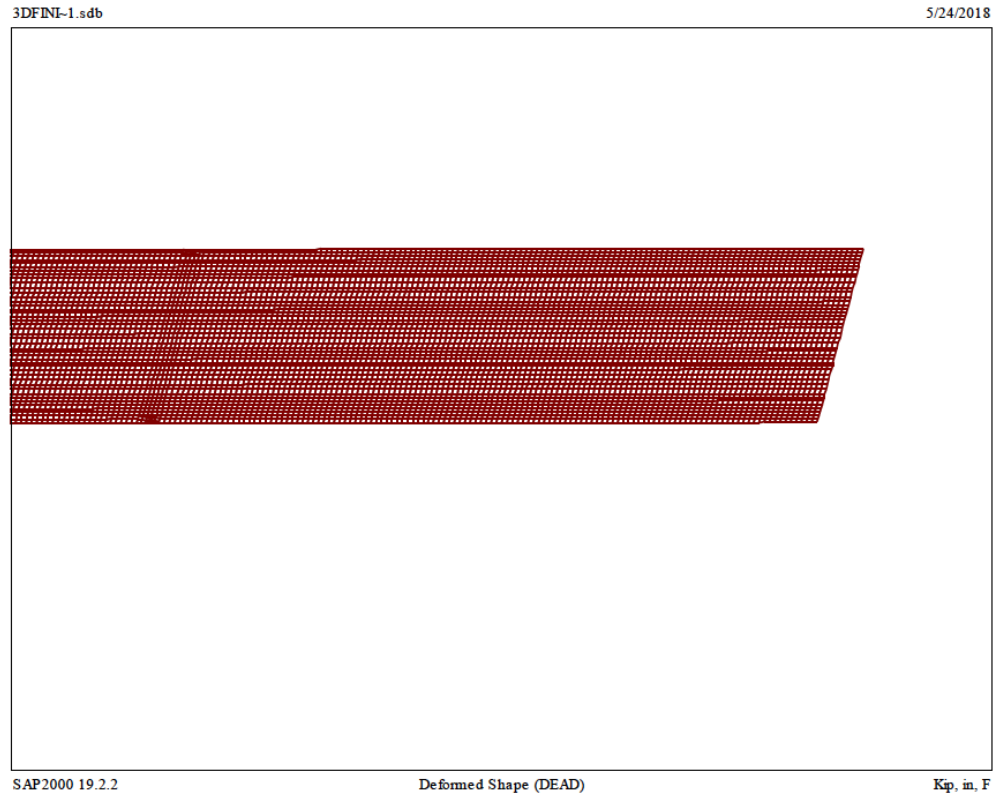
Figure 13. Typical elements of 12-in. mesh
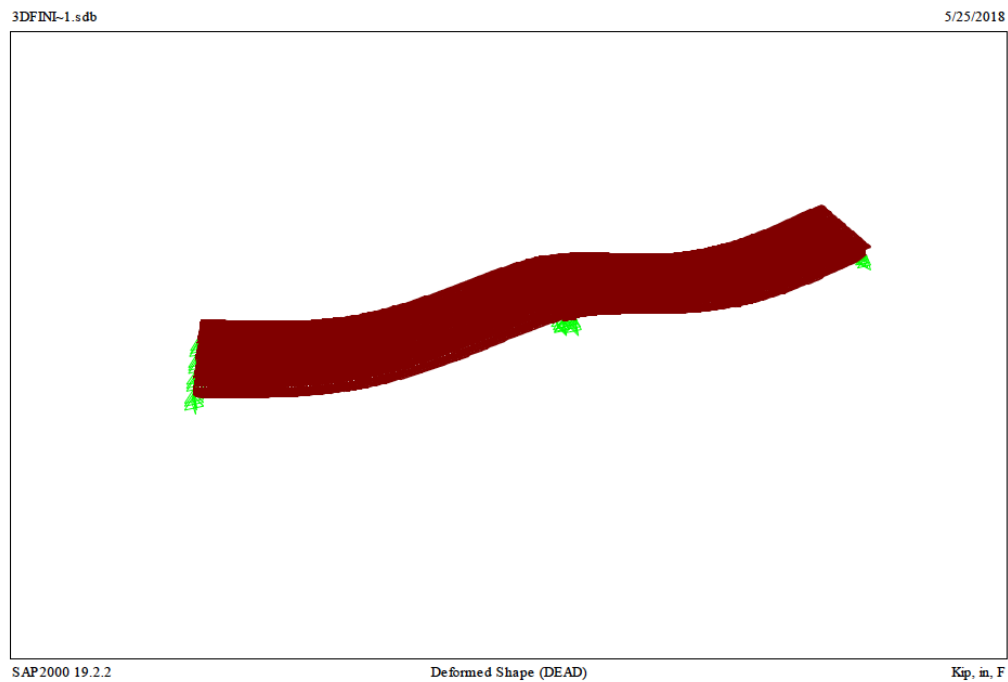
Figure 14. Deformation output of the bridge under self-weight

Table 8 summarizes the top and bottom strains in the bridge deck in the longitudinal and transverse directions at the six sensor tower locations that are estimated from the 3D FEM.

Table 8. Top and bottom strains in bridge deck at locations of six sensor towers
Longitudinal

Tower #	Concrete age (days)	Top strain (micro-strain)	Bottom strain (micro-strain)
1	3	1,050	260
1	56	1,150	420
1	260	1,090	400
2	3	1,050	260
2	56	1,150	420
2	260	1,090	400
3	3	350	170
3	56	400	200
3	260	610	220
4	3	2,000	1,100
4	56	2,250	1,200
4	260	2,350	1,220
5	3	1,050	300
5	56	1,150	500
5	260	1,350	600
6	3	1,100	800
6	56	1,150	850
6	260	1,250	950

Transverse

Tower #	Concrete age (days)	Top strain (micro-strain)	Bottom strain (micro-strain)
1	3	870	420
1	56	900	435
1	260	1,000	535
2	3	870	420
2	56	900	435
2	260	1,000	535
3	3	150	120
3	56	190	150
3	260	290	200
4	3	400	50
4	56	550	55
4	260	700	85
5	3	1,200	700
5	56	1,300	800
5	260	1,450	1,000
6	3	490	100
6	56	500	150
6	260	520	300

Figures 15 and 16 show the stress at the top of the bridge deck in the longitudinal and transverse directions, respectively. In the longitudinal direction, the stresses can reach the maximum positive values at the points of contact of the girder to the diaphragm. The stress decreases gradually along the bridge length to attain maximum negative values near mid-span. In the transverse direction, tensile stresses are shown to be positive near the diaphragm, which is due to the fact that the slab is acting as a top flange for the diaphragm. Away from the diaphragm, stresses are positive above the girders and negative in-between girders. The area where the six towers are located is under tension in the longitudinal and transverse directions.

The research team also performed another finite element analysis using the MIDAS software to verify the results obtained using the SAP2000 software. Solid elements were used to model the bridge compared to mesh elements in case of SAP2000. Unlike SAP2000, MIDAS allows

computing of average stresses on the entire slab section instead of computing the top and bottom

stress values in the bridge deck. However, this analysis was carried out to verify the distribution

of the stresses computed by SAP2000, which are discussed at this report.
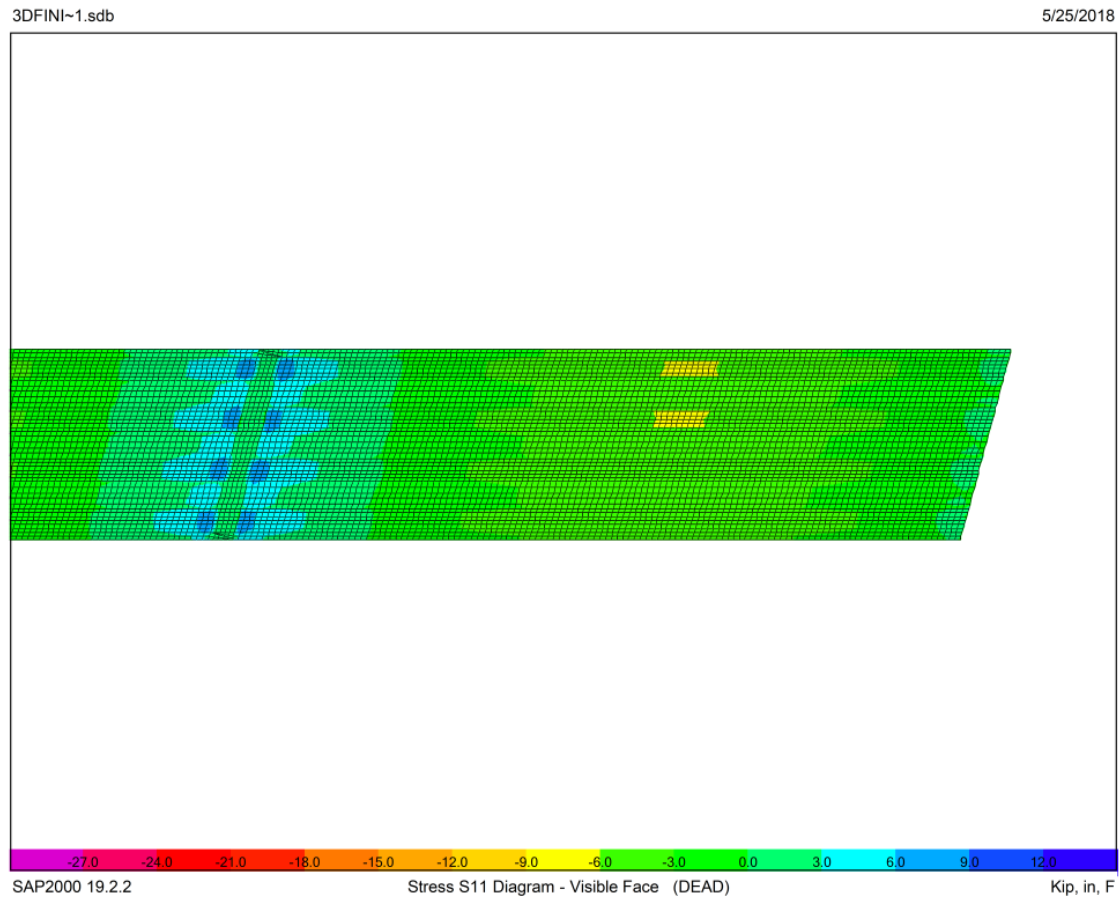
Figure 15. Stresses in longitudinal direction computed using SAP2000
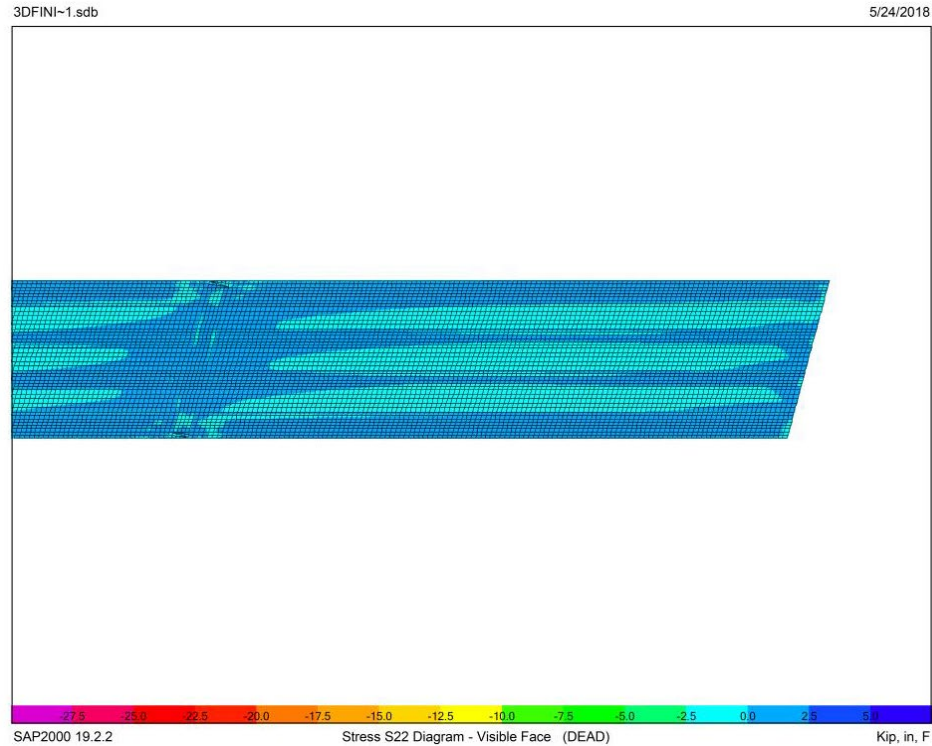
Figure 16. Stresses in transverse direction computed using SAP2000

Figures 17 and 18 show the average stress of the bridge deck that are computed using the MIDAS FEM in the longitudinal and transverse directions, respectively. In agreement with the SAP2000 FEM results, stresses in the longitudinal direction are shown to reach the maximum positive values at the points of contact of the girder to the diaphragm. These stresses decreased gradually along the bridge length to reach the maximum negative values near the mid-span of the bridge deck. The tensile stresses in the transverse direction are shown to be positive near the diaphragm. The stresses are positive above the girders and negative in-between girders in the transverse direction at sections away from the diaphragm. This resulted in the same stress pattern as results that was determined from the SAP2000 FEM, where the area under consideration where the six towers is under complete tension in the longitudinal and transverse directions.
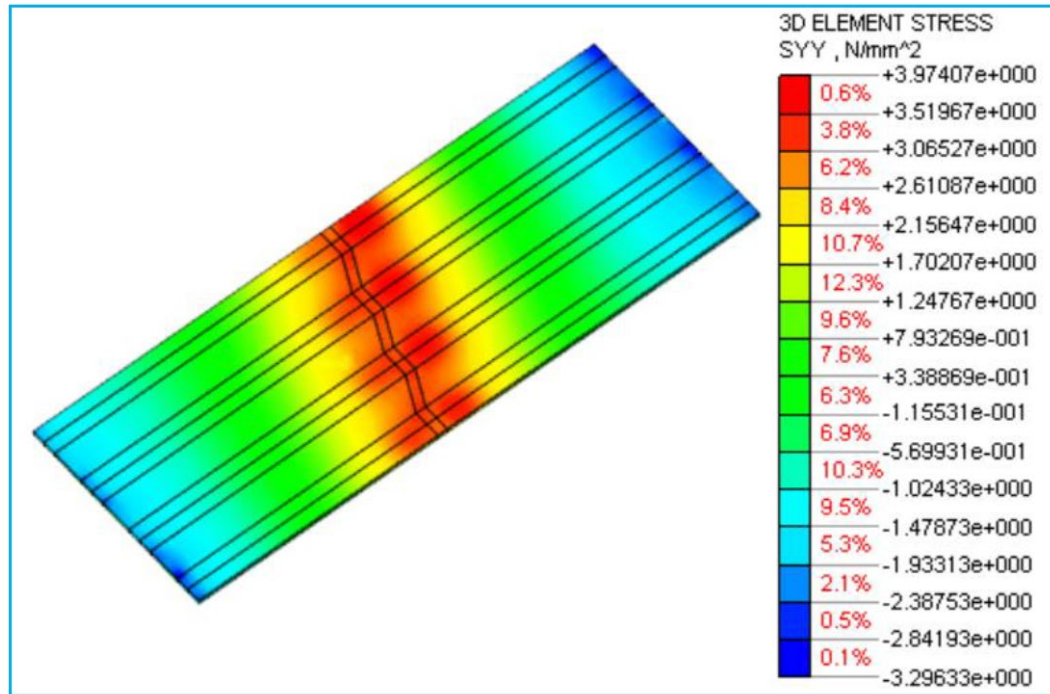
Figure 17 Stresses in longitudinal direction computed using MIDAS
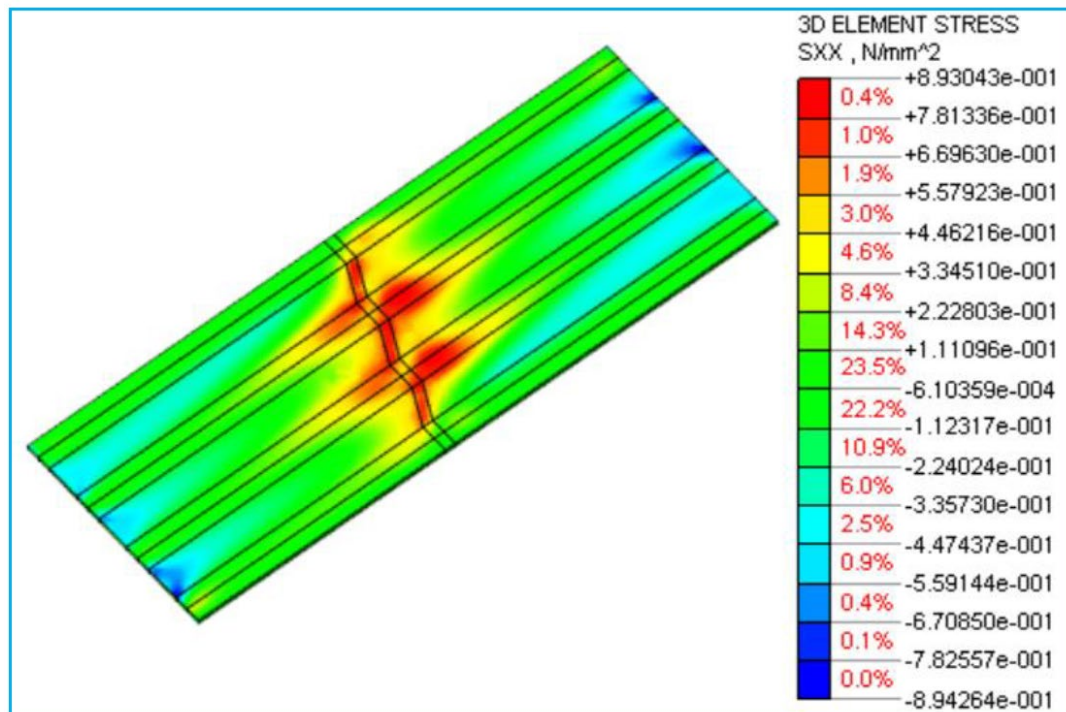
Figure 18 Stresses in transverse direction computed using MIDAS

9   STRAIN ANALYSIS

A strain model was proposed to evaluate strain data collected from the concrete embedded sensors. The model represents the total strain taken as the summation of strain values due to thermal deformation, concrete expansion or shrinkage, and structural deformation, as shown in Figure 19. Shrinkage strain can be computed from the laboratory testing of drying shrinkage (Figure 7). Thermal strains can be estimated by multiplying the temperature variations by the coefficient of thermal expansion. This value is taken to be $\frac{5}{9} \times 10^{-5} \frac{\mu in.}{in.}/°F$. The structural strain values were estimated from the FEM analysis and are reported in Table 8.

| Total Strain (Sensor Reading) | = | Shrinkage or Expansion (Lab results) | + | Thermal Strain (Calculated using thermocouple data) | + | Structural Strain (Computed from Finite Element Modeling) |
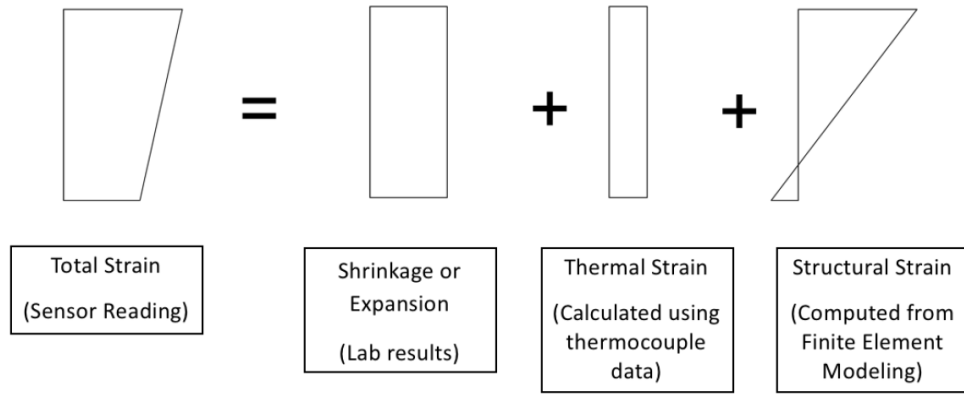
Figure 19. Proposed strain modeling for the bridge deck

The total strain from sensor readings can be estimated using Equation 1 as follow:

$$\varepsilon_{Sensor} = (\varepsilon_{dry} + \varepsilon_{30-36\ hrs}) + (\Delta\text{Temp} * \alpha) + (K * \varepsilon_{FEA}) \qquad (1)$$

where ε_{Sensor} is the strain from the sensor reading, ε_{dry} is the shrinkage strain calculated after 30-36 hours of age (time of demolding of shrinkage samples), $\varepsilon_{30-36\ hrs}$ is the shrinkage strain between the setting time of concrete and the time of demolding, ΔTemp is the temperature variation, α is the coefficient of thermal expansion, ε_{FEM} is the structural strain due to bridge self-weight (estimated using FEM, SAP2000), and K is the load distribution factor. This factor

represents the ratio between the portions of the load carried out by the concrete slab to the total load carried out by the slab, stay-in-place corrugated sheet formwork supporting the slab, and precast girders. The K value is expected to be close to zero when the concrete is plastic where all of the load is supported by the formwork and existing girders. The K factor increases thereafter towards 1. All parameters in Equation 1 are known previously from sensor data, FEM, and material properties measured in the lab, except for $\varepsilon_{30-36\ hrs}$ and K factor. In order to calculate these two unknown parameters, two methods were followed to solve Equation 1:

Method 1 – Applying Equation 1 at each strain reading separately assuming that the value of $\varepsilon_{30-36\ hrs}$ is zero. This will result in four values for the K factor at each sensor tower (K_1, K_2, K_3, and K_4) calculated using the strain values near the top and bottom of the concrete deck at each tower location under consideration in the longitudinal and transverse directions. After conducting this analysis, if the values of K_1 to K_4 are similar and lie between 0 and 1, the assumption that the concrete has no strain (autogenous shrinkage) at the time of demolding would be correct. Otherwise, the assumption can be judged to be wrong, and the second method needs to be followed where $\varepsilon_{30-36\ hrs} \neq 0$.

Method 2 – Applying Equation 1 at each tower separately in the longitudinal and transverse directions. The top and bottom strain values were used to solve Equation 1 at each sensor tower location, first in the longitudinal direction and then in the transverse direction in order to compute the two unknown values ($\varepsilon_{30-36\ hrs}$ and K). The outputs at each tower will be the load distribution factor in the longitudinal direction (K_L), in the load distribution factor in the transverse direction (K_T), and the two values for $\varepsilon_{30-36\ hrs}$, the average value of $\varepsilon_{30-36\ hrs}$ is considered in the analysis.

The age of concrete affects the structural strain since the elastic modulus of the concrete increases, hence resulting in higher K factor with more stress being transferred to the bridge deck. The expansion and shrinkage values also change with time. Thermal strain also changes due to variations in concrete temperature.

Equation 1 was applied at each tower in the longitudinal and transverse directions at three different ages (3, 56, and 260 days). Tables 9 to 18 summarize the model input and output data determined at Towers 1, 2, 3, 5, and 6, respectively. The sensors at Tower 4 were damaged during concrete placement operations. Figures 20 to 24 show the variations of the K factor with time in the longitudinal and transverse directions, as well as the average value for the deducted $\varepsilon_{30-36\,hrs}$ at each tower. Figure 25 shows the mean variations of the K factor with time in the longitudinal and transverse directions as well as the average value for the $\varepsilon_{30-36\,hrs}$ determined from the five remaining sensor tower locations. The results show that following Method 1 resulted in the same conclusion at the five sensor towers; that the values of K_1 to K_4 were not similar and did not yield values between 0 and 1. Therefore, the assumption that the concrete having no strain (autogenous shrinkage) at the time of demolding was wrong. Method 2 was then followed to compute K_L, K_T, and the average value of $\varepsilon_{30-36\,hrs}$. Values of K_L and K_T were close. The K values increased with concrete age with values around 0.7, 0.9, and 0.98 after 3, 56, and 260 days, respectively. The concrete shrinkage during the first 30-36 hours was estimated to be 74 micro-strain, which is consistent with the values found for similar mixtures in Reference 1.

Table 9. Model inputs for Tower 1

Tower 1	Tower 1	3 days	56 days	260 days
Measured properties	Elastic Modulus (ksi)	3660	3855	4100
Measured properties	Drying Shrinkage (micro-strain)	125	-185	-320
Measured properties	CTE (micro-strain/°F)	1.772×10^{-5}	1.772×10^{-5}	1.772×10^{-5}
Field Results (DAS)	Long. Top Strain (micro-strain)	1050	1150	1090
Field Results (DAS)	Long. Bottom Strain (micro-strain)	260	420	400
Field Results (DAS)	Trans. Top Strain (micro-strain)	870	900	1000
Field Results (DAS)	Trans. Bottom Strain (micro-strain)	420	435	535
Field Results (DAS)	Δ Temp (°F)	-45	-63	-81
Simulation Results (FEM)	Long. Top Strain (micro-strain)	1600	1790	1815
Simulation Results (FEM)	Long. Bottom Strain (micro-strain)	450	980	1115
Simulation Results (FEM)	Trans. Top Strain (micro-strain)	1460	1540	1725
Simulation Results (FEM)	Trans. Bottom Strain (micro-strain)	750	1010	1250

Table 10. Model outputs for Tower 1

Assuming $\varepsilon_{30-36\,hrs} = 0$

Tower 1	K_1 Long. Top	K_2 Long. Bottom	K_1 Trans. Top	K_2 Trans. Bottom
3 days	0.73	0.86	0.68	0.73
56 days	0.94	0.975	0.83	0.87
260 days	1.03*	1.05*	1.03*	1.04*

$\varepsilon_{30-36\,hrs} \neq 0$

Tower 1	Longitudinal K_L	Longitudinal $\varepsilon_{30-36\,hrs}$	Transverse K_T	Transverse $\varepsilon_{30-36\,hrs}$
3 days	0.69	75	0.63	70
56 days	0.90	72	0.88	84
260 days	0.985	71	0.980	81
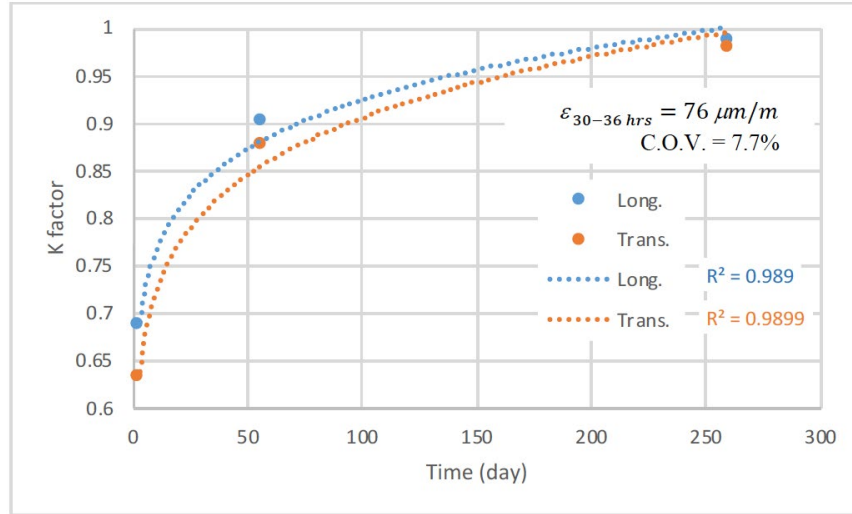
Figure 20. Values of K factor at Tower 1

Table 11. Model inputs for Tower 2

Tower 2	Tower 2	3 days	56 days	260 days
Measured properties	Elastic Modulus (ksi)	3660	3855	4100
Measured properties	Drying Shrinkage (micro-strain)	125	-185	-320
Measured properties	CTE (micro-strain/°F)	1.772×10^{-5}	1.772×10^{-5}	1.772×10^{-5}
Field Results (DAS)	Long. Top Strain (micro-strain)	350	400	610
Field Results (DAS)	Long. Bottom Strain (micro-strain)	170	200	220
Field Results (DAS)	Trans. Top Strain (micro-strain)	150	190	290
Field Results (DAS)	Trans. Bottom Strain (micro-strain)	120	150	200
Field Results (DAS)	Δ Temp (°F)	-45	-63	-81
Simulation Results (FEM)	Long. Top Strain (micro-strain)	570	956	1340
Simulation Results (FEM)	Long. Bottom Strain (micro-strain)	315	733	940
Simulation Results (FEM)	Trans. Top Strain (micro-strain)	286	722	1010
Simulation Results (FEM)	Trans. Bottom Strain (micro-strain)	243	678	917

Table 12. Model outputs for Tower 2

Assuming $\varepsilon_{30-36\,hrs} = 0$

Tower 2	K_1 Long. Top	K_2 Long. Bottom	K_1 Trans. Top	K_2 Trans. Bottom
3 days	0.83	0.94	0.96	0.44
56 days	0.98	1.00	1.00	1.01
260 days	1.03	1.05	1.05	1.06

$\varepsilon_{30-36\,hrs} \neq 0$

Tower 2	Longitudinal K_L	Longitudinal $\varepsilon_{30-36\,hrs}$	Transverse K_T	Transverse $\varepsilon_{30-36\,hrs}$
3 days	0.71	72.65	0.70	75.47
56 days	0.90	77.60	0.91	68.64
260 days	0.98	73.50	0.97	82.58
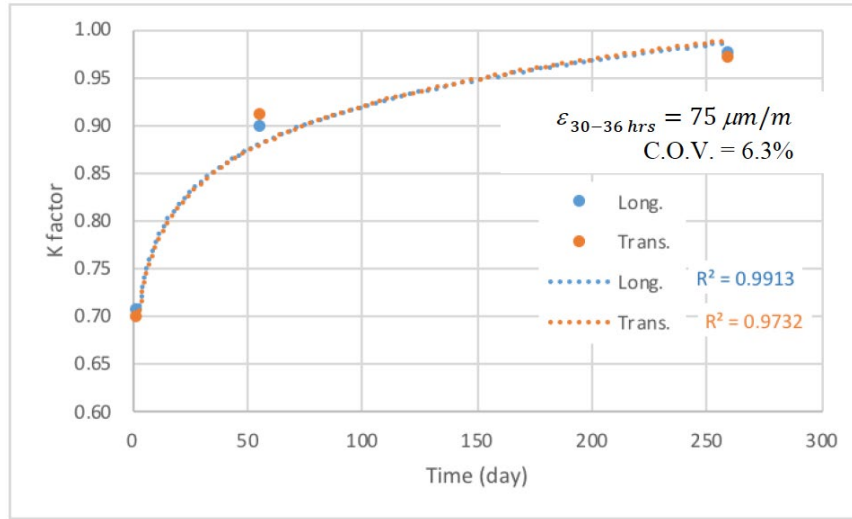
Figure 21. Values of K factor at Tower 2

Table 13. Model inputs for Tower 3

Tower 3	Tower 3	3 days	56 days	260 days
Measured properties	Elastic Modulus (ksi)	3660	3855	4100
Measured properties	Drying Shrinkage (micro-strain)	125	-185	-320
Measured properties	CTE (micro-strain/°F)	1.772×10^{-5}	1.772×10^{-5}	1.772×10^{-5}
Field Results (DAS)	Long. Top Strain (micro-strain)	2000	2250	2350
Field Results (DAS)	Long. Bottom Strain (micro-strain)	1100	1200	1220
Field Results (DAS)	Trans. Top Strain (micro-strain)	400	550	700
Field Results (DAS)	Trans. Bottom Strain (micro-strain)	50	55	85
Field Results (DAS)	Δ Temp (°F)	-45	-63	-81
Simulation Results (FEM)	Long. Top Strain (micro-strain)	2930	3011	3132
Simulation Results (FEM)	Long. Bottom Strain (micro-strain)	1640	1844	1965
Simulation Results (FEM)	Trans. Top Strain (micro-strain)	642	1122	1431
Simulation Results (FEM)	Trans. Bottom Strain (micro-strain)	143	572	800

Table 14. Model outputs for Tower 3

Assuming $\varepsilon_{30-36\,hrs} = 0$

Tower 3	K_1 Long. Top	K_2 Long. Bottom	K_1 Trans. Top	K_2 Trans. Bottom
3 days	0.73	0.75	0.82	0.60
56 days	0.92	0.94	0.97	1.03
260 days	1.00	1.01	1.03	1.07

$\varepsilon_{30-36\,hrs} \neq 0$

Tower 3	Longitudinal K_L	Longitudinal $\varepsilon_{30-36\,hrs}$	Transverse K_T	Transverse $\varepsilon_{30-36\,hrs}$
3 days	0.70	80.81	0.70	74.70
56 days	0.90	75.87	0.90	75.20
260 days	0.97	87.30	0.97	75.29
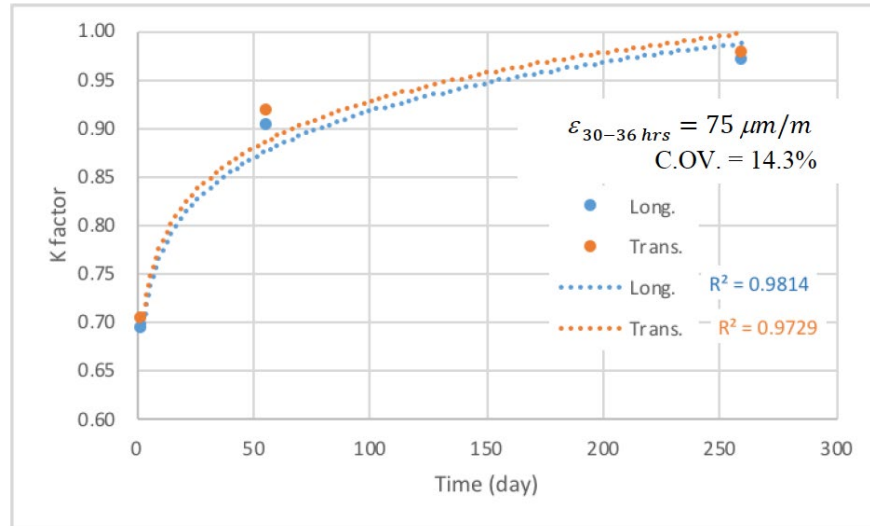
Figure 22. Values of K factor at Tower 3

Table 15. Model inputs for Tower 5

Tower 5	Tower 5	3 days	56 days	260 days
Measured properties	Elastic Modulus (ksi)	3660	3855	4100
Measured properties	Drying Shrinkage (micro-strain)	125	-185	-320
Measured properties	CTE (micro-strain/°F)	1.772×10^{-5}	1.772×10^{-5}	1.772×10^{-5}
Field Results (DAS)	Long. Top Strain (micro-strain)	1050	1150	1350
Field Results (DAS)	Long. Bottom Strain (micro-strain)	300	500	600
Field Results (DAS)	Trans. Top Strain (micro-strain)	1200	1300	1450
Field Results (DAS)	Trans. Bottom Strain (micro-strain)	700	800	1000
Field Results (DAS)	Δ Temp (°F)	-45	-63	-81
Simulation Results (FEM)	Long. Top Strain (micro-strain)	1575	1790	2100
Simulation Results (FEM)	Long. Bottom Strain (micro-strain)	505	1070	1330
Simulation Results (FEM)	Trans. Top Strain (micro-strain)	1790	1965	2190
Simulation Results (FEM)	Trans. Bottom Strain (micro-strain)	1080	1410	1730

Table 16. Model outputs for Tower 5

Assuming $\varepsilon_{30-36\ hrs} = 0$

Tower 5	K_1 Long. Top	K_2 Long. Bottom	K_1 Trans. Top	K_2 Trans. Bottom
3 days	0.75	0.84	0.74	0.73
56 days	0.94	0.97	0.93	0.95
260 days	1.01	1.03	1.01	1.02

$\varepsilon_{30-36\ hrs} \neq 0$

Tower 5	Longitudinal K_L	Longitudinal $\varepsilon_{30-36\ hrs}$	Transverse K_T	Transverse $\varepsilon_{30-36\ hrs}$
3 days	0.70	71.03	0.70	64.44
56 days	0.90	69.03	0.90	64.73
260 days	0.97	74.55	0.98	77.61
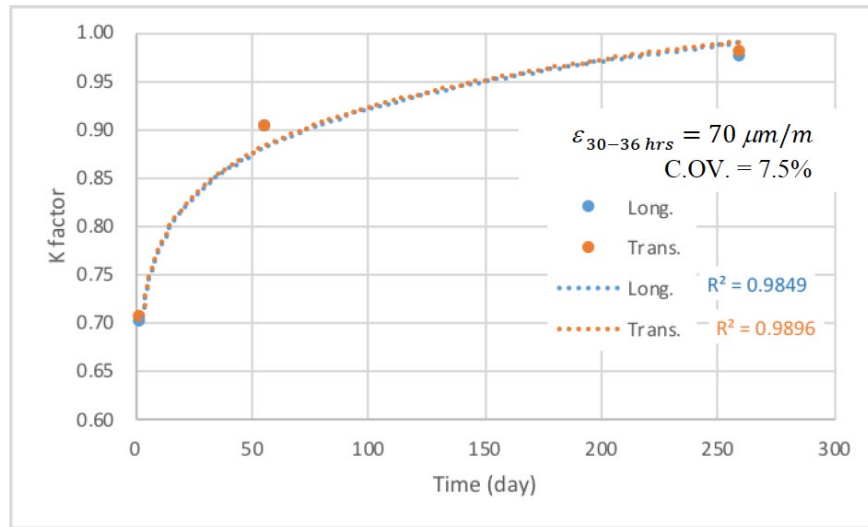
Figure 23. Values of K factor at Tower 5

Table 17. Model inputs for Tower 6

Tower 6	Tower 6	3 days	56 days	260 days
Measured properties	Elastic Modulus (ksi)	3660	3855	4100
Measured properties	Drying Shrinkage (micro-strain)	125	-185	-320
Measured properties	CTE (micro-strain/°F)	1.772×10^{-5}	1.772×10^{-5}	1.772×10^{-5}
Field Results (DAS)	Long. Top Strain (micro-strain)	1100	1150	1250
Field Results (DAS)	Long. Bottom Strain (micro-strain)	800	850	950
Field Results (DAS)	Trans. Top Strain (micro-strain)	490	500	520
Field Results (DAS)	Trans. Bottom Strain (micro-strain)	100	150	300
Field Results (DAS)	Δ Temp (°F)	-45	-63	-81
Simulation Results (FEM)	Long. Top Strain (micro-strain)	1640	1790	1985
Simulation Results (FEM)	Long. Bottom Strain (micro-strain)	1210	1460	1680
Simulation Results (FEM)	Trans. Top Strain (micro-strain)	775	1060	1245
Simulation Results (FEM)	Trans. Bottom Strain (micro-strain)	215	670	1020

Table 18. Model outputs for Tower 6

Assuming $\varepsilon_{30-36\,hrs} = 0$

Tower 6	K_1 Long. Top	K_2 Long. Bottom	K_1 Trans. Top	K_2 Trans. Bottom
3 days	0.75	0.76	0.79	0.59
56 days	0.94	0.95	0.98	1.02
260 days	1.02	1.02	1.04	1.05

$\varepsilon_{30-36\,hrs} \neq 0$

Tower 6	Longitudinal K_L	Longitudinal $\varepsilon_{30-36\,hrs}$	Transverse K_T	Transverse $\varepsilon_{30-36\,hrs}$
3 days	0.70	80.81	0.70	75.27
56 days	0.91	57.73	0.90	83.72
260 days	0.98	67.54	0.98	72.67
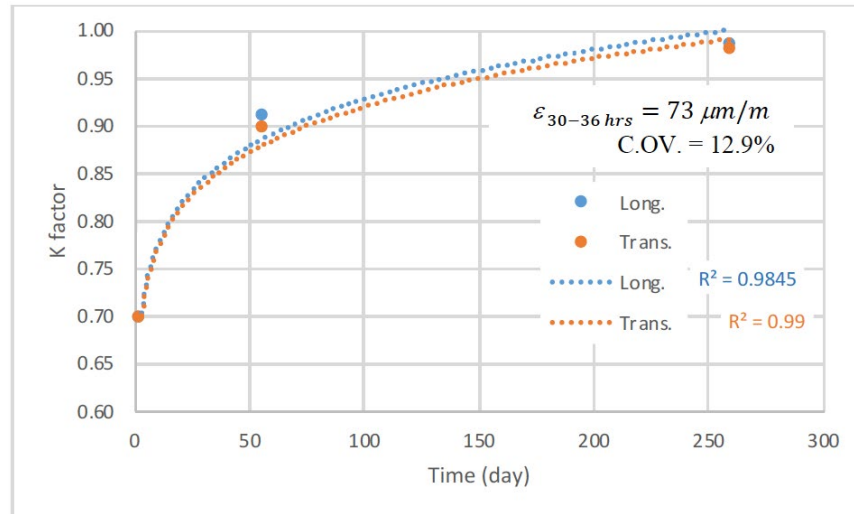
Figure 24. Values of K factor at Tower 6
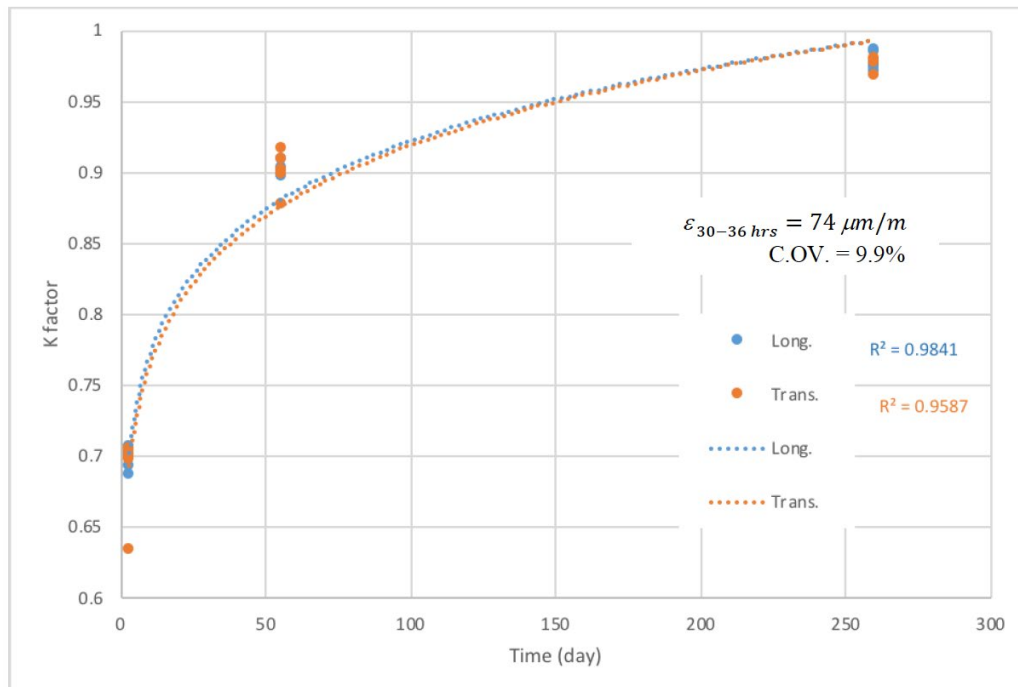
Figure 25. Values of K factor using all towers data

10   FIELD INSPECTION

A field inspection was carried out shortly before the preparation of this report, after approximately 10 months of the bridge construction. No signs of cracking were observed except for hairline cracks that appeared in the bridge deck around the intermediate bent where the six sensor towers were located. The cracks were within the area where the girders' continuity stops, and the maximum tensile strengths took place, as illustrated from the FEMs discussed earlier. The cracks were noticed to be within 18 ft to the East and West sides of the central diaphragm. The strain gauges did not show any sudden drop in concrete strain, which reflects that the depth of the cracking was limited.

A detailed inspection of the bridge deck will be carried out in collaboration with MoDOT to survey and to measure crack lengths and widths as well as any other defects in the concrete. The results of the field inspection will be submitted to MoDOT as soon as the survey is finished.

11   LIFE CYCLE AND COST ANALYSIS

The following section is based on the report that was developed in collaboration with the research team of Dr. Kaan Ozbay of New York Poly, who is a co-PI in the RE-CAST Tier-1 National University Transportation Center [2] [3].

Performing a life cycle and cost analysis (LCCA) is a strategic decision-support approach for selecting the best new construction material. The benefits of using the new FRC material can include: 1) cost-effectiveness and longer service life of the innovative construction material; 2) the more efficient use of resources and energy in construction operations; and 3) the use of construction methodologies that will minimize construction duration and reduce traffic delays [4] [5].

Since the proposed FRC had better mechanical properties, lower shrinkage, and improved cracking resistance than conventional concrete used for similar re-decking of bridges, a longer service life with less anticipated frequency of maintenance and repair is anticipated. Service life for a structure is determined when the structure reaches a certain conditional rating. The relationship between time and conditional rating of a structure is named deterioration function.

Two approaches namely, deterministic approach and probabilistic approach, can be applied in the LCCA procedure. Although deterministic approach is computationally simpler, it usually fails to accurately capture the underlying high level of uncertainty of the input parameters by only considering a single fixed value of parameters and may result in a misleading judgment of decision makers. The outcome is more amplified in transportation projects due to the long lifetime of these projects once built. For example, two possible values of a material's unit price may lead to two different decisions in terms of choosing one alternative over the other one. Besides material unit price, other input parameters such as the discount rate, are usually subject

to different levels of uncertainty as well. Realizing this drawback of using the deterministic approach, the FHWA has been encouraging the use of LCCA probabilistic approach (FHWA 2002)[6]. Moreover, the probabilistic LCCA is highly recommended when dealing with innovative materials and construction technologies since the uncertainties from the limited field data demand the use of such a probabilistic approach.

Two reference bridges are considered in this study. The first reference bridge (Bridge 2) is a similar bridge that was cast using conventional vibrated concrete (CVC) and located at Route 13 over Log Creek near Kingston , MO. It is a two span bridge measuring 120 ft and 124 ft and has a width of 30 ft. Both the Taos bridge (Bridge 1) and Bridge 2 have one travel lane in each direction. The second reference bridge (Bridge 3) is considered at an area of higher traffic volume in order to evaluate the effect of high traffic on the LCCA. Bridge 3 is in state of New Jersey at I-80 that is located 0.7 miles east of the Passaic River. This bridge was cast using CVC as well.

The input information is based on estimated costs and material properties collected for conventional concrete and FRC from field implementation as well as laboratory results. The estimated cost of the FRC was $446/yd^2 in March 2017 and the estimated cost of the reference conventional concrete was $334/yd^2 in February 2016. Both values were converted into 2018 dollars in the case study. Longer service life is accepted because of higher mechanical properties, higher durability, lower shrinkage, higher ductility, and higher crack resistance.

11.1 Deterministic LCCA

Multiple scenarios with different service lives and traffic volume conditions are evaluated for the deterministic LCCA (Table 19). Two low traffic volume scenarios using information from the FRC bridge located at Taos (Bridge 1) with an average daily traffic (ADT) of 668

vehicles and the conventional concrete bridge located on Route 13 (Bridge 2) with an ADT of 3387 are considered. One high traffic volume scenario using a bridge located on I-80 near Passaic River, New Jersey (Bridge 3), which is a benchmark for high traffic volume brides in LCCA, with an ADT of 114,739 is evaluated as well. For low volume scenarios, flagging work zone operation with a reduced capacity of 200 vehicles per lane per hour (State of New Jersey Department of Transportation 2015) is assumed. Traffic growth rate is assumed to be 1% for the low volume scenarios and 0.5% for the high volume scenario. Analysis period is set to 120 years to ensure at least one rehabilitation activity for each alternative will be included in the proposed LCCA. Discount rate is assumed as 3% according to one of the previous reports in Missouri (Bledsoe, Sadasivam, and Mallela 2013) [7]. Only work zone related user and social costs are considered. Due to the limitation of the data availability, only air pollution cost is included in social cost. To not dominate total life cycle costs, user cost is multiplied by a weighted factor (0.3 in this example) when calculating the sum of all individual costs into total life cycle cost (LCC) for High Volume Scenario.

For Low Volume Scenario 1, since the hourly traffic volume never exceeds our assumed work zone reduced capacity (200 vehs/lane/hour), traffic delay cost and vehicle operation costs are zero (no queues) and crash risk cost is close to zero (Figure 26 (a)). Therefore, user and social costs are very small compared with agency costs. By contrast, high volume scenario has significantly higher values in terms of user cost as work zone activities have significant impacts on road users in terms of traffic delay and vehicle operation (Figure 26 (c)).
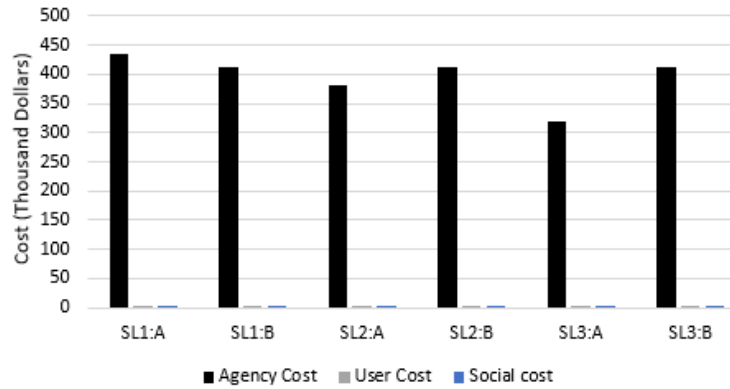
(a) Low Volume Scenario 1 (668 ADT)
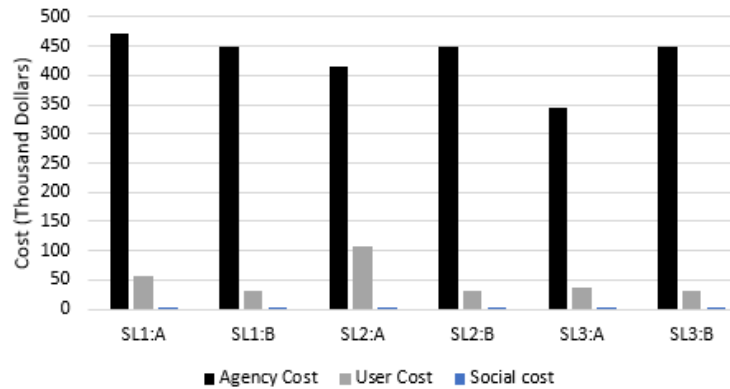
(b) Low Volume Scenario 2 (3,387 ADT)
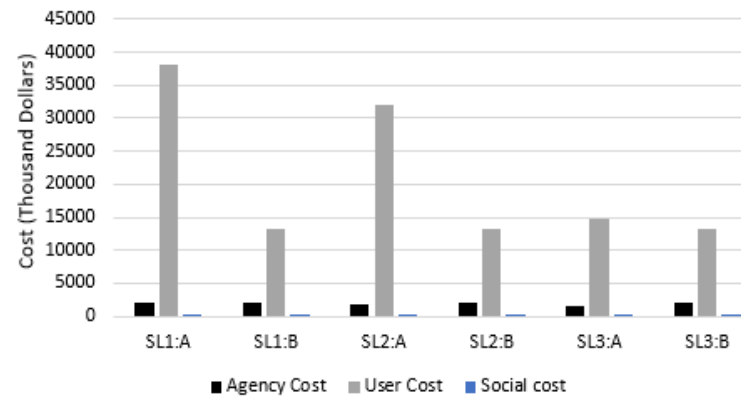
(c) High Volume Scenario (114,739 ADT)

Figure 26. Deterministic LCCA Results

Table 19. Deterministic LCCA Scenarios

Service Life Scenario	Conventional Concrete Service Life (Year)	FRC Service Life (Year)
Service Life Scenario 1 (SL1)	40	75
Service Life Scenario 2 (SL2)	50	75
Service Life Scenario 3 (SL3)	75	75

Traffic Volume Scenario	ADT	Truck%
Low Traffic Volume Scenario 1	668	5%
Low Traffic Volume Scenario 2	3,387	22%
High Traffic Volume Scenario	114,739	1.55%

Table 20 shows the detailed values of agency, user, social and total LCC for each scenario. In general, the agency costs of the two alternatives (Alternative A is conventional concrete, Alternative B is FR-C) can be considered as equivalent since their difference is less than 10% in Service Life Scenarios 1 & 2. A cost break down for Service Life Scenario 1 in Low Volume Scenario 2 shows that Alternative B FRC has a relatively lower discounted rehabilitation cost ($59,379) compared to that of Alternative A ($168,093). However, as the initial construction cost of the new material is still higher compared to that of the conventional material, the difference of the final agency cost of the two alternatives are relatively small.

FRC has cost savings in terms of user and social cost in all scenarios. It should be noted that although the percentage of cost savings are high in Low Volume Scenario 1, the absolute values of the costs are actually small because of the low traffic volume (668 ADT). When calculating the total LCC by summing up agency, user and social cost, Alternative B FRC can have a cost saving up to 56% in High Volume Scenario. However, in Service Life Scenario 3, Alternative A conventional concrete has a lower agency and total life cycle cost compared to those of FRC. This is because both alternatives have the same service life (75 years) in this scenario, but FRC has a much higher construction unit price.

The results indicate that one of the biggest advantages of using FRC is the user cost savings (i.e. less traffic delay, shorter work zone duration), especially for bridges with high traffic volumes. However, for bridges with very low ADT, benefits in terms of user costs are very small.

Table 20. Summary of the deterministic LCCA Results

Low Volume Scenario 1

Service Life Scenario 1	Alt A (40 Years)	Alt B (75 Years)	Alt B Benefit
Agency Cost	$435,300	$412,900	5%
User Cost	$306	$95	69%
Social cost	$68	$21	69%
LCC	$435,674	$413,016	5%

Service Life Scenario 2	Alt A (50 Years)	Alt B (75 Years)	Alt B Benefit
Agency Cost	$382,000	$412,900	-8%
User Cost	$238	$95	60%
Social cost	$53	$21	60%
LCC	$382,291	$413,016	-8%

Service Life Scenario 3	Alt A (75 Years)	Alt B (75 Years)	Alt B Benefit
Agency Cost	$318,000	$412,900	-30%
User Cost	$106	$95	10%
Social cost	$24	$21	13%
LCC	$318,130	$413,016	-30%

Low Volume Scenario 2

Service Life Scenario 1	Alt A (40 Years)	Alt B (75 Years)	Alt B Benefit
Agency Cost	$472,000	$447,800	5%
User Cost	$56,722	$32,300	43%
Social cost	$351	$109	69%
LCC	$529,073	$480,209	9%

Service Life Scenario 2	Alt A (50 Years)	Alt B (75 Years)	Alt B Benefit
Agency Cost	$414,200	$447,800	-8%
User Cost	$108,024	$32,300	70%
Social cost	$272	$109	60%
LCC	$522,496	$480,209	8%

Service Life Scenario 3	Alt A (75 Years)	Alt B (75 Years)	Alt B Benefit
Agency Cost	$344,800	$447,800	-30%
User Cost	$35,889	$32,300	10%
Social cost	$121	$109	10%
LCC	$380,810	$480,209	-26%

High Volume Scenario

Service Life Scenario 1	Alt A (40 Years)	Alt B (75 Years)	Alt B Benefit
Agency Cost	$2,170,200	$2,058,700	5%
User Cost	$38,252,100	$13,242,500	65%
Social cost	$8,700	$2,400	72%
Weighted LCC*	$13,654,530	$6,033,850	56%

Service Life Scenario 2	Alt A (50 Years)	Alt B (75 Years)	Alt B Benefit
Agency Cost	$1,904,500	$2,058,700	-8%
User Cost	$32,053,300	$13,242,500	59%
Social cost	$6,400	$2,400	63%
Weighted LCC	$11,526,890	$6,033,850	48%

Service Life Scenario 3	Alt A (75 Years)	Alt B (75 Years)	Alt B Benefit
Agency Cost	$1,585,300	$2,058,700	-30%
User Cost	$14,713,800	$13,242,500	10%
Social cost	$2,700	$2,400	11%
Weighted LCC	$6,002,140	$6,033,850	-1%

* To not dominate total life cycle costs, user cost is multiplied by a weighted factor (0.3 in this example) when calculating the sum of all individual costs (Holland 2012) for High Volume Scenario.

11.2 Probabilistic LCCA

Instead of using deterministic values for all input parameters, probabilistic approach is strongly recommended especially due to the use of the new-technology material with limited field data that is studied in this project. Stochastic treatment for the input parameters, such as Monte Carlo simulation method, is needed in this approach. Monte Carlo simulation is a powerful technique that has been widely used in many disciplines, and often the simplest way to perform probabilistic analysis. The core idea of the Monte Carlo simulation method is to learn about a highly stochastic system by simulating it through the use of the random sampling method. The Monte Carlo approach uses randomly selected values for input parameters with uncertainty based on the probability of a certain value occurring for a specific parameter according to a pre-specified probability distribution. Then, it obtains the system response for this randomly generated input vector and records the value of the system response (Jawad 2003) [8]. This process is performed repetitively until the desired level of accuracy is reached. The system response value from each iteration will be used to construct the probability distribution of the final outcome which is the LCC in our case. Such a probabilistic approach will provide evaluation of multiple variable inputs including costs, service lives, and economic factors to estimate the likelihood of the estimated life cycle cost.

The first step in the probabilistic approach is to identify the input parameters with uncertainty. In this case study, parameters such as traffic growth rate, discount rate, improvement rate of the new material in terms of service life are considered as not having fixed deterministic values.

11.3 Stochastic variation of a single input parameter

In order to observe the impact of each probabilistic input parameter on the total life cycle cost, variation of a single parameter approach is suggested. For example, since the proposed FR-SWC will have better material properties such as higher mechanical properties, higher durability, lower shrinkage, higher ductility, and higher crack resistance, a longer service life is expected. The estimated improvement rate on service life are obtained by assigning weights to the degree of improvement of each material property. The following list summarizes the degree of improvement of the FRC compared to conventional bridge deck concrete in percentage. By assigning weights for key performance criteria (Shrinkage: 0.2, Cracking potential: 0.3, Splitting Tensile Strength: 0.2, Compressive Strength: 0.15 , Elastic Modulus: 0.15), we have an estimated improvement rate of service life (98%) for FR-SWC.

- 1-year shrinkage: 20% (710 vs. 570 micro-strain)

- Cracking potential: 220% time of cracking from restrained shrinkage test (12.5 vs. 39.5 days)

- Flexural strength: 30% (650 vs. 845 psi at 56 d)

- Toughness: 1900% (0.6 vs. 12.2 ft.lb at 56 d)

- Compressive Strength: 22% (7,700 vs, 6,300 psi at 56 d)

- Splitting Tensile Strength: 125% (420 vs, 940 psi at 56 d)

- Elastic Modulus 56-day: 2% (3,775 vs, 3,855 ksi at 56 d)

With limited field implementation, the new material construction cost can be highly uncertain. It is assumed that the estimated improvement rate of FRC in terms of the extended service life follows a Triangular distribution $Tri(50\%, 98\%, 118\%)$ with a most likely value of 98%. This corresponds to a service life of the FRC bridge ranges from 60 years to 83 years

with a most likely value of 79 years. We also assume a more stable service life variation of the conventional concrete that follows a Triangular distribution $Tri(40, 42.5, 45)$. By performing random sampling approach using Monte Carlo simulation technique, we can estimate the probability density function (PDF) and cummulative distribution fucntion (CDF) of the costs for each alternative. For example, the following figure shows the PDF and CDF for agency cost and LCC using information from Bridge 2 (low traffic volume with 3,387 ADT). The probabilistic results with 5000 runs indicate an 80% chance that the FR-SWC alternative will have a lower agency cost and 100% chance that the FR-SWC alternative will have a lower total LCC compare to conventional concrete alternative.
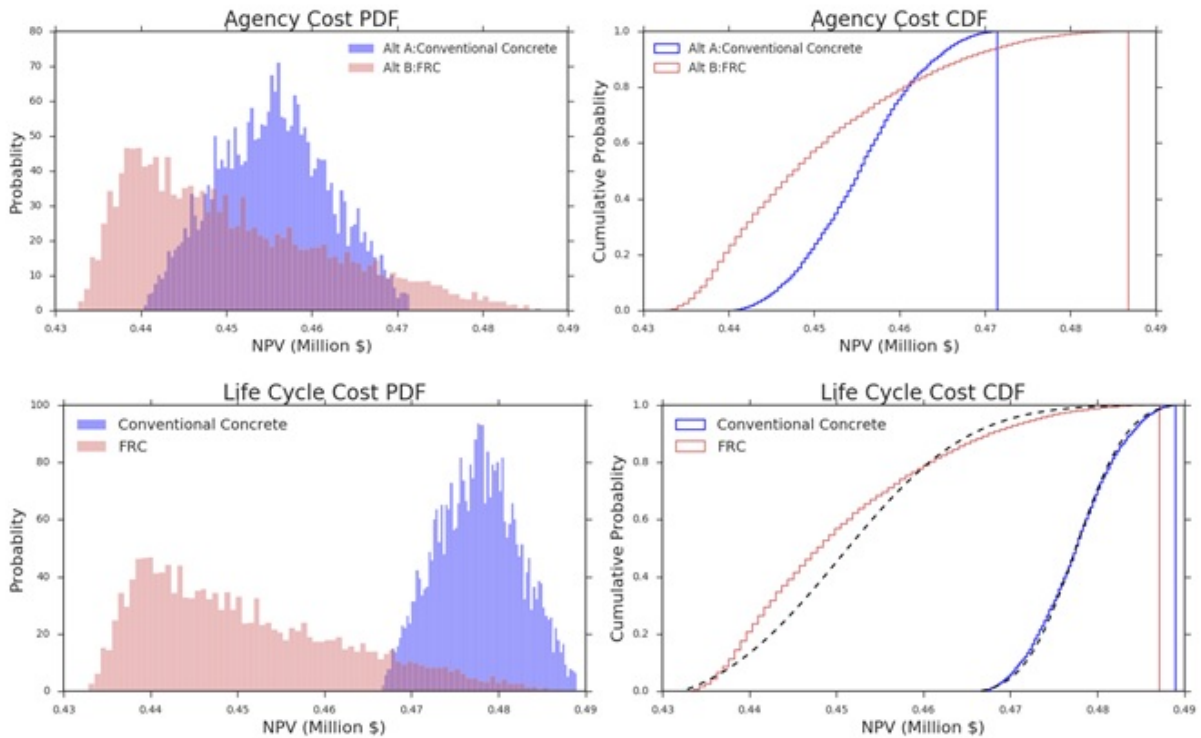
Figure 27. Estimated Agency Cost and LCC using Probabilistic Service Life

11.4 Stochastic variation of multiple parameters

If more than one input parameter are treated probabilistically, the final output will be a combination of all the effects from random distributions of these parameters. For instance, if

we determine that the discount rate, service life and traffic growth rate have high uncertainties and also assume that they have the distributions shown in Table 21, the total life cycle cost of the two alternatives are estimated as shown in Figure 27. The mean or most likely values for the distributions are based on information obtained from RE-CAST 3A Phase I project. The standard deviation and lower or upper bound of these parameters are obtained through project team discussion or best estimates.

Table 21. Probabilistic approach input parameters and their distributions

Parameter	Alternative A	Alternative B
Discount Rate	Normal, $N(3\%,\ 1\%)$	Normal, $N(3\%,\ 1\%)$
Service Life	Triangular, $Tri(40,42.5,45)$	Triangular, $Tri(60,\ 79.2,\ 83.2)$
Traffic Growth Rate	Normal, $N(1.5\%,\ 0.5\%)$	$N(1.5\%,\ 0.5\%)$

Figure 28 illustrates total LCC with stochastic variations in one or multiple input parameters using information from Bridge 2 (low traffic volume with 3,387 ADT). This probabilistic approach allows the investigation of the impacts of each input parameter. Moreover, it also provides the sensitivity of the final LCC when using multiple probabilistic input parameters. For example, Figure 28 implies that the variations in discount rate may have the biggest impacts on the total LCC as Figure 28 (a) and (d) share similar shape in terms of their PDFs.
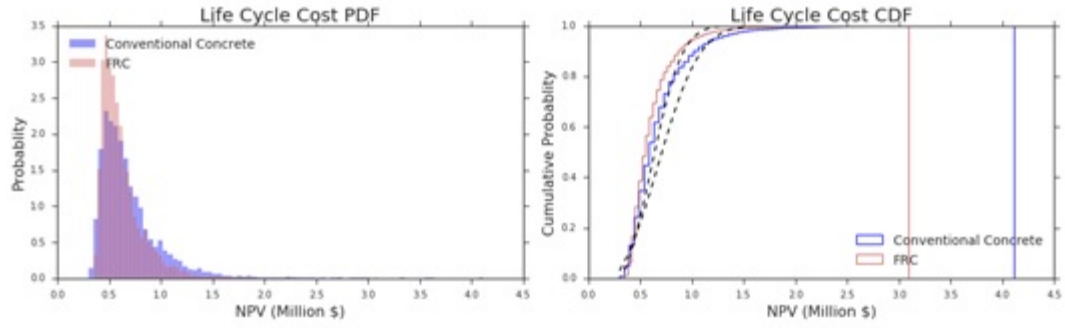
(a) Total Life Cycle Cost with Variations in Discount Rate
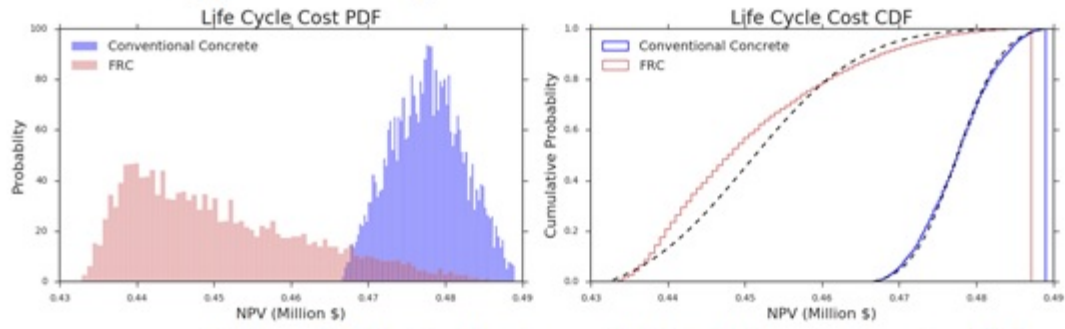
(b) Total Life Cycle Cost with Variations in Service Life
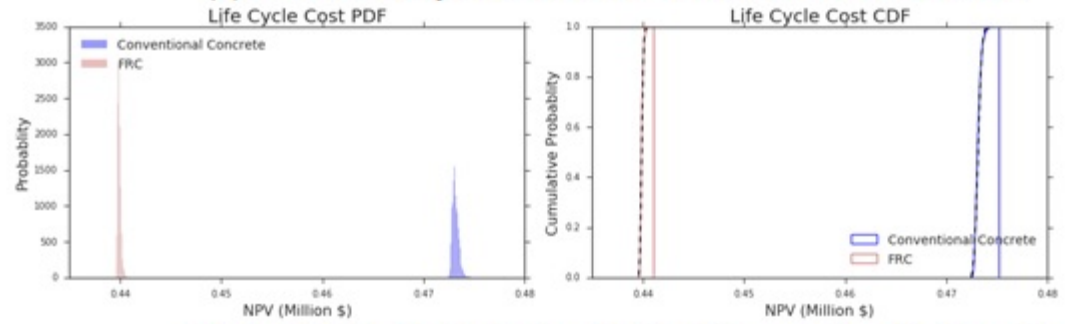
(c) Total Life Cycle Cost with Variations in Traffic Growth
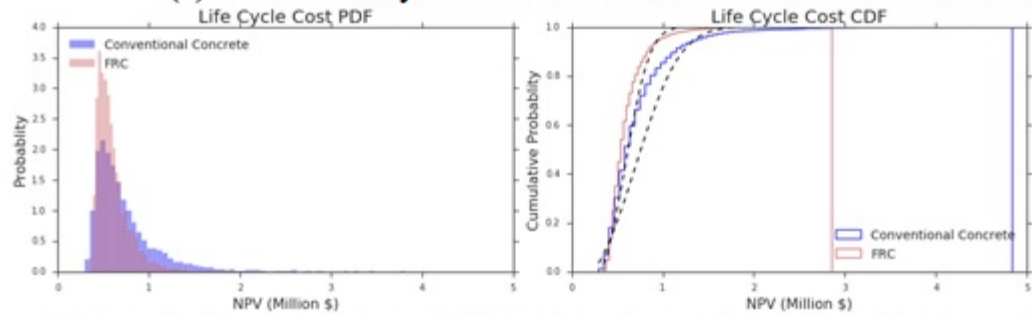
(d) Total Life Cycle Cost with Stochastic Variations in All Three Parameters

Figure 28. Total Life Cycle Cost with variations in one or multiple input parameters

Table 22 summarizes the probabilistic outputs with stochastic variations of all three input parameters. Although the material unit cost of the proposed FR-SCC is more expensive than the reference conventional material ($446/yd^2 compare to $334/yd^2), both alternatives have similar mean values for the agency cost. In terms of indirect out-of-pocket cost, the proposed FRC alternative has significant benefits over the conventional material. The output shows that the proposed FRC has 44.73% cost savings when compared with the mean values of user costs of the conventional concrete material. This yields a 17.02% cost savings in terms of the total life cycle (Table 22). The probability distribution functions and cumulative distribution functions of the total LCC for the two alternatives are shown in Figure 28 (d). The CDF of the total LCC also indicates that the probability that the conventional concrete alternative has a lower LCC than the FR-SCC alternative is only 20%.

Table 22. Probabilistic outputs with variations of all three parameters

| Costs	Mean (dollars)	Standard deviation (dollars)	Alt B Benefit %
Agency Cost (Alt A)	488,300	130,300	
Agency Cost (Alt B)	474,000	89,800	2.93%
User Cost (Alt A)	824,553	84,358	
User Cost (Alt B)	455,714	42,109	44.73%
Social Cost (Alt A)	532	355	
Social Cost (Alt B)	213	180	59.96%
Total Life Cycle Cost (Alt A)	736,200	380,300	
Total Life Cycle Cost (Alt B)	610,900	208,700	17.02%

As clearly depicted in this case study, in the case of conventional concrete based bridge, both deterministic and probabilistic results indicate a slightly lower or equal agency and total life cycle costs compared with low volume bridges built with FRC. For high volume bridges, the proposed FRC based construction alternative has a significant benefit in terms of user cost that leads to a lower total life cycle cost when compared with that of conventional concrete

alternative. Although deterministic LCCA approach provides straightforward evaluations of both alternatives, probabilistic LCCA approach can also be an effective tool for a risk-based decision-making process due to high uncertainties of the new material. The probabilistic approach can also be extended as the sensitivity analysis that can help identify certain chosen parameters for evaluating various different alternatives.

12   CONCLUSIONS

Based on the results presented in this report, the following conclusions can be drawn:

1. The proposed FRC was successfully used for casting of the bridge deck, near Taos, Missouri. The concrete exhibited high workability and was easily pumped into place, consolidated, and finished.

2. The proven FR-SWC intended for the construction of bridge substructure elements with a targeted slump flow of 20 in. was modified for the casting of the bridge deck by reducing the dosage rate of the HRWRA to limit the slump value to 8 ± 2 in. for the construction of the bridge deck. This was necessary to hold the crown slope of the bridge deck in the transverse direction (2%).

3. A mock-up slab measuring 10×10 ft was prepared with tight reinforcing bars and 2% slope in the transverse direction. The results indicated the necessity to lower the concrete slump to prevent any settlement over the crown and control the concrete temperature to enhance placement and finishing.

4. Concrete sampled at the end of the pumpline on the jobsite that took place in late July 2017 had slump values of 6-10 in. and air content of 5.5% to 7%. Ice was added for the last 26 of the 40 truck deliveries needed to complete the job to reduce the concrete temperature from 97 to 85°F.

5. Concrete was sampled from three different trucks to evaluate mechanical properties and shrinkage. The mean compressive strengths at 28 and 56 days were 6,450 and 7,770 psi, respectively. The mean splitting tensile strengths at 28 and 56 days were 940 and 1,010 psi, respectively. The mean 56-day flexural strength was 845 psi. The mean elastic modulus values at 3 and 56 days were 3,660 and 3,855 ksi.

61

6. The concrete exhibited an initial expansion of 125 micro-strain after 7 days of age, corresponding to the end of moist curing. The concrete had shrinkage thereafter. The concrete designed with relatively low w/cm and an expansive agent had a relatively low shrinkage values of 185 and 320 micro-strain after 56 and 260 days, respectively, of drying.

7. A comprehensive program involving 108 sensors was undertaken to evaluate in-situ properties of the concrete, including temperature, relative humidity, and strain. Six sensor towers were installed within 18 ft to the East and to the West sides of the intermediate bent. High tensile strain of up to 2,100 micro-strain were obtained at the intersection of the intermediate bent with one of the pre-cast concrete girders.

8. Two 3D finite element models were developed using SAP2000 and MIDAS to estimate structural strain in the concrete deck due to the bridge's own weight. Unlike SAP2000, MIDAS allows computing an average stress on the entire slab section instead of computing the top and bottom stress values that can be attained with the former model. The results from both models showed that the area under consideration near the intermediate bent, where the six towers are located, is under tension in the longitudinal and transverse directions.

9. A strain model was proposed to evaluate the strain data collected from the embedded sensors. The model was used to evaluate strains and estimate values of the concrete shrinkage during the first 30-36 hours, corresponding to the time of demolding of the shrinkage samples. Load distribution factor, which is the ratio between the portion of the load carried out by the concrete slab to the total load carried out by the slab and the stay-in-place corrugated sheet formwork material as well as the precast girders,

was also estimated from the model. Findings indicated that the load distribution factor increased with concrete age to reach 0.98 at 260 days. The average concrete shrinkage during the first 30-36 hours was estimated to be 75 micro-strain.

10. A field inspection was carried out shortly before the preparation of this report after approximately 10 months of the casting of the bridge deck. No signs of cracking were observed in the deck except for hairline cracks that appeared near the intermediate bent where the six sensor towers were located. The cracks were within girders' continuity stops where maximum tensile strengths were expected, and verified from the two finite element models.

11. LCCA was performed to estimate the LCC savings of using the FRC in bridge deck construction compared to regular bridge deck made with CVC in scenarios involving low and high traffic volume conditions. The analysis indicated that the use of FRC can provide cost savings for both user and social costs for the low and high traffic volume scenarios. It should be noted that although the percentage of cost savings is high in the case of the low volume scenario, the absolute values of the costs are actually small because of the low traffic volume (e.g., 668 ADT). When calculating the total LCC by summing up the agency, user, and social costs, the use of FRC was shown to provide a cost saving of up to 55% for the high traffic volume scenario.

REFERENCES

[1]   Khayat, K.H. and Abdelrazik, A. (2017) "Performance of Fiber-Reinforced Self-Consolidating Concrete for Repair of Bridge Sub-Structures and Fiber-Reinforced Super-Workable Concrete for Infrastructure Construction," Report cmr17-012, Missouri Department of Transportation, 196 pp.

[2]   Gao, J., Ozbay, K., Nassif, H, and Kalan, O. (2019) "Stochastic Multi-Objective Optimization-Based Life Cycle Cost Analysis for New Construction Materials and Technologies" Transportation Research Board 98th Annual Meeting, Washington, D.C.

[3]   Gao, J., and Ozbay, K., (pending) "Life Cycle Cost Analysis for Research on Concrete Applications for Sustainable Transportation (RE-CAST)". New York University C2SMART Center.

[4]   Kaan, O., Yanmaz-Tuzel, O. Mudigonda, S., Bartin, B., and Berechman, J. (2007) "Cost of Transporting People in New Jersey-Phase II, " New Jersey Department of Transportation Final Report. Report No FHWA/NJ-2007-003.

[5]   Lou, P., Nassif, H., Su, D., and Truban, P. (2016) "Effect of Overweight Trucks on Bridge Deck Deterioration Based on Weigh-in-Motion Data," Journal of the Transportation Research Board, 2592: 86-97.

[6]   FHWA (2002) "Life-Cycle Cost Analysis Primer," 25 pp.

[7]   Bledsoe, James, Suri Sadasivam, and Jagannath Mallela. 2013. "Missouri Demonstration Project: Replacement of Three Bridges Using Hybrid-Composite Beam Technology."

[8]   Jawad, J. (2003). "Life Cycle Cost Optimization for Infrastructure Facilities" Doctoral Thesis, Rutgers University.

APPENDIX

Sensor Wiring Codifications

Station 1 (Distance between sensor location to bridge edge at diaphragm 10.5 ft)

Gauge Type/number	Color	Code	DAS Wiring input	Wire Length (ft)	Foot Marker Start	Foot Marker End
Concrete 1 Long.	White	1-C-1	1 in Set (1-16)	22	2234	2256
Concrete 2 Long.	White	1-C-2	2 in Set (1-16)	22	2256	2278
Concrete 3 Long.	White	1-C-3	3 in Set (1-16)	22	2278	2300
Concrete 4 Trans.	Yellow	1-C-4	4 in Set (1-16)	22	2300	2322
Concrete 5 Trans.	Yellow	1-C-5	5 in Set (1-16)	22	2322	2344
Concrete 6 Trans.	Yellow	1-C-6	6 in Set (1-16)	22	2344	2366
Rebar 1 Long.	Blue	1-R-1	7 in Set (1-16)	24	2366	2390
Rebar 2 Long.	Blue	1-R-2	8 in Set (1-16)	24	2390	2414
Rebar 3 Long.	Blue	1-R-3	9 in Set (1-16)	24	2414	2438
Rebar 4 Trans.	Red	1-R-4	10 in Set (1-16)	24	2438	2462
Rebar 5 Trans.	Red	1-R-5	11 in Set (1-16)	24	2462	2486
Rebar 6 Trans.	Red	1-R-6	12 in Set (1-16)	24	2486	2510
Humidity 1	Green	1-H-1	1 in Set (Humid)	22	2510	2532
Humidity 2	Green	1-H-2	2 in Set (Humid)	22	2532	2554
Humidity 3	Green	1-H-3	3 in Set (Humid)	22	2554	2576
Thermocouple 1	Orange	1-T-1	1 in Set (Temp)	22	-	-
Thermocouple 2	Orange	1-T-2	2 in Set (Temp)	22	-	-
Thermocouple 3	Orange	1-T-3	3 in Set (Temp)	22	-	-

Station 2 (Distance between sensor location to bridge edge at diaphragm 7 ft)

Gauge Type/number	Color	Code	DAS Wiring input	Wire Length (ft)	Foot Marker Start	Foot Marker End
Concrete 1 Long.	White	2-C-1	1 in Set (49-64)	18	3852	3870
Concrete 2 Long.	White	2-C-2	2 in Set (49-64)	18	3870	3888
Concrete 3 Long.	White	2-C-3	3 in Set (49-64)	18	3888	3906
Concrete 4 Trans.	Yellow	2-C-4	4 in Set (49-64)	18	3906	3924
Concrete 5 Trans.	Yellow	2-C-5	5 in Set (49-64)	18	3924	3942
Concrete 6 Trans.	Yellow	2-C-6	6 in Set (49-64)	18	3942	3960
Rebar 1 Long.	Blue	2-R-1	7 in Set (49-64)	20	3960	3980
Rebar 2 Long.	Blue	2-R-2	8 in Set (49-64)	20	3980	4000
Rebar 3 Long.	Blue	2-R-3	9 in Set (49-64)	20	4000	4020
Rebar 4 Trans.	Red	2-R-4	10 in Set (49-64)	20	4020	4040
Rebar 5 Trans.	Red	2-R-5	11 in Set (49-64)	20	4040	4060
Rebar 6 Trans.	Red	2-R-6	12 in Set (49-64)	20	4060	4080
Humidity 1	Green	2-H-1	13 in Set (Humid)	18	4080	4098
Humidity 2	Green	2-H-2	14 in Set (Humid)	18	4098	4116
Humidity 3	Green	2-H-3	15 in Set (Humid)	18	4116	4134
Thermocouple 1	Orange	2-T-1	13 in Set (Temp)	18	-	-
Thermocouple 2	Orange	2-T-2	14 in Set (Temp)	18	-	-
Thermocouple 3	Orange	2-T-3	15 in Set (Temp)	18	-	-

Station 3 (Distance between sensor location to bridge edge at diaphragm 14 ft)

Gauge Type/number	Color	Code	DAS Wiring input	Wire Length (ft)	Foot Marker Start	Foot Marker End
Concrete 1 Long.	White	3-C-1	13 in Set (49-64)	24	148	172
Concrete 2 Long.	White	3-C-2	14 in Set (49-64)	24	172	196
Concrete 3 Long.	White	3-C-3	15 in Set (49-64)	24	196	220
Concrete 4 Trans.	Yellow	3-C-4	16 in Set (49-64)	24	220	244
Concrete 5 Trans.	Yellow	3-C-5	1 in Set (65-80)	24	244	268
Concrete 6 Trans.	Yellow	3-C-6	2 in Set (65-80)	24	268	292
Rebar 1 Long.	Blue	3-R-1	3 in Set (65-80	26	292	318
Rebar 2 Long.	Blue	3-R-2	4 in Set (65-80)	26	318	344
Rebar 3 Long.	Blue	3-R-3	5 in Set (65-80)	26	344	370
Rebar 4 Trans.	Red	3-R-4	6 in Set (65-80)	26	370	396
Rebar 5 Trans.	Red	3-R-5	7 in Set (65-80)	26	396	422
Rebar 6 Trans.	Red	3-R-6	8 in Set (65-80)	26	422	448
Humidity 1	Green	3-H-1	16 in Set (Humid)	24	448	472
Humidity 2	Green	3-H-2	17 in Set (Humid)	24	472	496
Humidity 3	Green	3-H-3	18 in Set (Humid)	24	496	520
Thermocouple 1	Orange	3-T-1	16 in Set (Temp)	24	-	-
Thermocouple 2	Orange	3-T-2	17 in Set (Temp)	24	-	-
Thermocouple 3	Orange	3-T-3	18 in Set (Temp)	24	-	-

Station 4 (Distance between sensor location to bridge edge at diaphragm 19.5 ft)

Gauge Type/number	Color	Code	DAS Wiring input	Wire Length (ft)	Foot Marker Start	Foot Marker End
Concrete 1 Long.	White	4-C-1	9 in Set (17-32)	30	2918	2948
Concrete 2 Long.	White	4-C-2	10 in Set (17-32)	30	2948	2978
Concrete 3 Long.	White	4-C-3	11 in Set (17-32)	30	2978	3008
Concrete 4 Trans.	Yellow	4-C-4	12 in Set (17-32)	30	3008	3038
Concrete 5 Trans.	Yellow	4-C-5	13 in Set (17-32)	30	3038	3068
Concrete 6 Trans.	Yellow	4-C-6	14 in Set (17-32)	30	3068	3098
Rebar 1 Long.	Blue	4-R-1	15 in Set (17-32)	32	3098	3130
Rebar 2 Long.	Blue	4-R-2	16 in Set (17-32)	32	3130	3162
Rebar 3 Long.	Blue	4-R-3	1 in Set (33-48)	32	3162	3194
Rebar 4 Trans.	Red	4-R-4	2 in Set (33-48)	32	3194	3226
Rebar 5 Trans.	Red	4-R-5	3 in Set (33-48)	32	3236	3268
Rebar 6 Trans.	Red	4-R-6	4 in Set (33-48)	32	3268	3300
Humidity 1	Green	4-H-1	7 in Set (Humid)	30	3300	3330
Humidity 2	Green	4-H-2	8 in Set (Humid)	30	3330	3360
Humidity 3	Green	4-H-3	9 in Set (Humid)	30	3360	3390
Thermocouple 1	Orange	4-T-1	7 in Set (Temp)	30	-	-
Thermocouple 2	Orange	4-T-2	8 in Set (Temp)	30	-	-
Thermocouple 3	Orange	4-T-3	9 in Set (Temp)	30	-	-

Station 5 (Distance between sensor location to bridge edge at diaphragm 19.5 ft)

Gauge Type/number	Color	Code	DAS Wiring input	Wire Length (ft)	Foot Marker Start	Foot Marker End
Concrete 1 Long.	White	5-C-1	5 in Set (33-48)	30	3390	3420
Concrete 2 Long.	White	5-C-2	6 in Set (33-48)	30	3450	3480
Concrete 3 Long.	White	5-C-3	7 in Set (33-48)	30	3420	3450
Concrete 4 Trans.	Yellow	5-C-4	8 in Set (33-48)	30	3480	3510
Concrete 5 Trans.	Yellow	5-C-5	9 in Set (33-48)	30	3510	3540
Concrete 6 Trans.	Yellow	5-C-6	10 in Set (33-48)	30	3540	3570
Rebar 1 Long.	Blue	5-R-1	11 in Set (33-48)	32	3570	3602
Rebar 2 Long.	Blue	5-R-2	12 in Set (33-48)	32	3602	3634
Rebar 3 Long.	Blue	5-R-3	13 in Set (33-48)	32	3634	3666
Rebar 4 Trans.	Red	5-R-4	14 in Set (33-48)	32	3666	3698
Rebar 5 Trans.	Red	5-R-5	15 in Set (33-48)	32	3698	3730
Rebar 6 Trans.	Red	5-R-6	16 in Set (33-48)	32	3730	3762
Humidity 1	Green	5-H-1	10 in Set (Humid)	30	3762	3792
Humidity 2	Green	5-H-2	11 in Set (Humid)	30	3792	3822
Humidity 3	Green	5-H-3	12 in Set (Humid)	30	3822	3852
Thermocouple 1	Orange	5-T-1	10 in Set (Temp)	30	-	-
Thermocouple 2	Orange	5-T-2	11 in Set (Temp)	30	-	-
Thermocouple 3	Orange	5-T-3	12 in Set (Temp)	30	-	-

Station 6 (Distance between sensor location to bridge edge at diaphragm 10.5 ft)

Gauge Type/number	Color	Code	DAS Wiring input	Wire Length (ft)	Foot Marker Start	Foot Marker End
Concrete 1 Long.	White	6-C-1	13 in Set (1-16)	22	2620	2642
Concrete 2 Long.	White	6-C-2	14 in Set (1-16)	22	2598	2620
Concrete 3 Long.	White	6-C-3	15 in Set (1-16)	22	2576	2598
Concrete 4 Trans.	Yellow	6-C-4	16 in Set (1-16)	22	2642	2664
Concrete 5 Trans.	Yellow	6-C-5	1 in Set (17-32)	22	2664	2686
Concrete 6 Trans.	Yellow	6-C-6	2 in Set (17-32)	22	2686	2708
Rebar 1 Long.	Blue	6-R-1	3 in Set (17-32)	24	2708	2732
Rebar 2 Long.	Blue	6-R-2	4 in Set (17-32)	24	2732	2756
Rebar 3 Long.	Blue	6-R-3	5 in Set (17-32)	24	2756	2780
Rebar 4 Trans.	Red	6-R-4	6 in Set (17-32)	24	2780	2804
Rebar 5 Trans.	Red	6-R-5	7 in Set (17-32)	24	2804	2828
Rebar 6 Trans.	Red	6-R-6	8 in Set (17-32)	24	2828	2852
Humidity 1	Green	6-H-1	4 in Set (Humid)	22	2852	2874
Humidity 2	Green	6-H-2	5 in Set (Humid)	22	2874	2896
Humidity 3	Green	6-H-3	6 in Set (Humid)	22	2896	2918
Thermocouple 1	Orange	6-T-1	4 in Set (Temp)	22	-	-
Thermocouple 2	Orange	6-T-2	5 in Set (Temp)	22	-	-
Thermocouple 3	Orange	6-T-3	6 in Set (Temp)	22	-	-